

# Benchmarking and contrasting exchange-correlation functional differences in response to static correlation in unrestricted Kohn-Sham and a hybrid 1-electron reduced density matrix functional theory

Daniel Gibney and Jan-Niklas Boyn\*

*Department of Chemistry, University of Minnesota, Minneapolis, Minnesota 55455, United States*

(Dated: April 14, 2025)

A hybrid Kohn-Sham Density Functional Theory (KS-DFT) and 1-electron Reduced Density Matrix Functional Theory (1-RDMFT) has recently been developed to describe strongly correlated systems at mean-field computational cost. This approach relies on combining a Reduced Density Matrix Functional to capture strong correlation effects with existing exchange correlation (XC) functionals to capture the remaining dynamical correlation effects. In this work, we systematically benchmark the performance of nearly 200 different XC functionals available within LibXC in this DFA 1-RDMFT framework, contrasting it with their performance in unrestricted KS-DFT. We identify optimal XC functionals for use within DFA 1-RDMFT and elucidate fundamental trends in the response of different XC functionals to strong correlation in both DFA 1-RDMFT and UKS-DFT.

## I. INTRODUCTION

Kohn-Sham Density Functional Theory (KS-DFT) has become one of the most widely available and utilized methods in computational chemistry over the past 30 years[1–4]. This widespread adoption is due to its low computational scaling of  $\mathcal{O}(N^3)$ , enabling it to treat systems that are intractable for wavefunction-based methods, in combination with the relatively high accuracy of modern exchange correlation (XC) functionals. [5–11] However, the exact XC functional is unknown and therefore approximations are used in its place. This results in significant variation in the accuracy of DFT calculations, depending on the underlying XC functional utilized and the system being considered.[12] Examples of common issues with which XC functionals are known to struggle include the treatment of charge transfers and strongly correlated systems, as well as a notable electron self-interaction error.[13–15]

Due to the aforementioned errors and the near-ubiquity of DFT, a large number of XC functionals have been constructed over the years. These are broadly categorized using a Jacob’s ladder style classification scheme, introduced by Perdew in 2001.[16] Jacob’s ladder classifies XC functionals according to the amount of information included in the functional. As one ascends the rungs, functionals, in theory, become more accurate. In ascending order, the first three rungs of Jacob’s ladder are Local Spin Density Approximations (LSDAs), which rely only on the electron density, Generalized Gradient Approximations (GGAs), which include the gradient of the electron density, and Meta-Generalized Gradient Approximations (mGGAs), which include the kinetic energy density. Further rungs are presented by Hybrid and Range Separated Hybrid (RSH) functionals,

which include exact Hartree-Fock (HF) exchange, and Double Hybrids, which introduce a wavefunction-based correlation energy correction, usually in the form of a perturbation method.[17, 18]

The construction of functionals on any rung of Jacob’s ladder generally falls into two different schools of thought.[19] The most common approach is to optimize the functional parameters using chemical systems to reproduce known accurate experimental or theoretical values, yielding empirical functionals. A significant difficulty with this approach is collecting a large and varied swath of accurate reference data to optimize the functional, as only using a limited number of systems and properties may result in a functional with limited applicability outside of the properties optimized on. Commonly used examples of functionals developed in this way include the Minnesota class of functionals, e.g., M06-L, M11-L, MN12-L, MN15-L.[20–23] It has been noted that modern functional development with its focus on reproducing chemical properties has resulted in a degradation of the fundamental quantity of DFT, the electron density, suggesting that some functional improvements are the result of overfitting and do not present better approximations to the exact functional.[24, 25] The other approach to functional construction is to accurately reproduce and obey known physical properties and conditions that the unknown exact functional must satisfy, yielding non-empirical or ab-initio functionals. Examples of functionals constructed in this way that are commonly utilized include TPSS, revTPSS, and SCAN.[26–28]

A significant challenge for DFT is the capture of static (also referred to as strong or multi-reference correlation), which is characterized by multiple Slater determinants contributing significantly to the wavefunction. These effects are difficult to capture via improvements to the functional as they are non-local in nature.[29] Due to this difficulty and the high computational scaling of

---

\* jboyn@umn.edu

systematically improvable wavefunction-based alternatives, significant efforts have been made to develop methodologies that can capture strong correlation effects while still utilizing existing XC functionals. These include the breaking of spin symmetry, allowing the alpha and beta electrons to occupy different spatial orbitals (spin-unrestricted or broken-symmetry DFT (UKS-DFT)), [30–33] enforcing the Perdew–Parr–Levy–Baldur (PPLB) flat-plane conditions with fractional spins and charges to recover the piece wise linearity between integer numbers of electrons, [34–36] as well as utilizing complex and hyper-complex numbers to create fractionally occupied orbitals while still maintaining a single Slater determinant reference. [37–40] The latter two approaches both utilize fractional orbital occupations in capturing the strong correlation effects.

An alternative to DFT or the more expensive wavefunction based approaches for describing electron correlation is provided by 1-electron Reduced Density Matrix (1-RDM) Functional Theory (1-RDMFT). This class of methods aims to capture strong electron correlation through fractional occupations of the 1-RDM. [41–55] 1-RDMFTs have previously shown success in describing band gaps of semiconductors and Mott insulators, both of which DFT struggles with. [56, 57] Natural Orbital Functional Theory (NOFT) is a related approach, in which natural orbitals and their occupation numbers are used in place of the 1-RDM to reconstruct the 2-RDM subject to N-representability conditions. [50, 54, 58–60] Unfortunately, both of these approaches require expensive orbital optimizations under orthogonality constraints limiting the sizes of systems they can be applied to. [61] However, since these approaches use the 1-RDM as their fundamental variables, they are naturally suited to describing strong correlation through fractional occupation numbers.

In a similar vein, we have previously developed a DFA 1-RDMFT that combines the strengths of 1-RDMFTs to capture strong correlation through the 1-RDM with standard XC functionals, which are well suited for capturing dynamical correlation. [62–65] This formulation allows us to inherit the favorable computational scaling of the utilized DFA, as well as its accuracy in non-strongly-correlated systems, through recovering DFT’s energy, while significantly improving upon it in the presence of strong correlation. Additionally, as strong correlation is recovered through the 1-RDM, no unphysical breaking of spin-symmetry, as is the case in UKS, occurs.

As currently available XC functionals are not designed with DFA 1-RDMFT in mind, our goal is to work toward the creation of a task-specific functional designed to perform well within the DFA 1-RDMFT framework. Here, the aim is to have the XC functional recover dynamical correlation while the 1-RDM correction captures strong correlation. To this end, we expand

upon previous work, [63–65] which focused on developing the DFA 1-RDMFT methodology and its derivation through exploration of the XC functional dependence in the DFA 1-RDMFT framework by benchmarking nearly 200 XC functionals. This large scope, spanning the rungs of Jacob’s ladder, allows us to elucidate trends in functional response to multi-reference character and identify general scaling parameters,  $\kappa$  (*vide infra*), for a large class of functionals commonly used today. Here, the value of  $\kappa$ , correlates with the magnitude of the correction required for a specific functional to recover strong correlation effects through the 1-RDM term. We compare the functional errors obtained using both UKS-DFT and DFA 1-RDMFT to uncover any functional relationships between the two. Finally, the relationship between DFA 1-RDMFT and HF exchange is explored through systematic modification of hybrid XC functionals.

## II. THEORY

The DFA 1-RDMFT energy is defined as

$$E_{1\text{RDMFT}}[{}^1D] = E_{\text{DFT}}[{}^1D] + \tilde{w}\text{Tr}({}^1D^2 - {}^1D). \quad (1)$$

The first term,  $E_{\text{DFT}}[{}^1D]$ , is the traditional DFT energy expressible as:

$$E_{\text{DFT}}[{}^1D] = T_s[{}^1D] + V[\rho] + F_{xc}[\rho], \quad (2)$$

with  $T_s$  being the non-interacting kinetic energy,  $V[\rho]$  being the energy from the electron-electron, electron-nuclei, and nuclei-nuclei columbic energies, and  $F_{XC}[\rho]$  being the XC energy. The second term,  $\tilde{w}\text{Tr}({}^1D^2 - {}^1D)$ , is the 1-RDM functional, which we derived previously from the first term in the unitary decomposition of the 2-electron reduced density matrix’s cumulant contribution to the electronic energy. [63, 64] We have shown previously that this term corresponds primarily to strongly correlated electronic interactions, due to it only including the diagonal terms in the 2-RDMs cumulant. [63, 66]  $\tilde{w}$  above is defined as

$$\tilde{w} = \frac{\kappa\text{Tr}({}^2I)}{\text{Tr}({}^2W^2I)} \sum_{ij} (2\langle ij|ij\rangle - \langle ij|ji\rangle), \quad (3)$$

where

$$\text{Tr}({}^2W^2I) = 4 \sum_{\tilde{i}<\tilde{j}} \tilde{W}_{\tilde{i}\tilde{j}} + \sum_{\tilde{i}} \tilde{W}_{\tilde{i}\tilde{i}}, \quad (4)$$

$$\tilde{W}_{\tilde{i}\tilde{j}} = \frac{\langle \tilde{i}\tilde{j}|\tilde{i}\tilde{j}\rangle}{\sqrt{\langle \tilde{i}\tilde{i}|\tilde{i}\tilde{i}\rangle \langle \tilde{j}\tilde{j}|\tilde{j}\tilde{j}\rangle}}, \quad (5)$$

and

$$\text{Tr}({}^2I) = \frac{r(r-1)}{2}. \quad (6)$$

Here,  $r$  denotes the number of spin orbitals,  $i$  and  $j$  run over the spatial orbitals,  $\tilde{i}$  and  $\tilde{j}$  run over the atomic orbitals, and  $\kappa$  is a functional specific scaling parameter between 0 and 1. The overall 1-RDMFT energy inherits DFTs non-linearity in  ${}^1D$  and it must therefore be obtained via a self-consistent field procedure with the objective function minimized at each iteration being:

$$\min \text{Tr}({}^1H_{KS}[{}^1D]{}^1D) + \tilde{w}\text{Tr}({}^1D^2 - {}^1D), \quad (7)$$

where  ${}^1H_{KS}$  is the Kohn-Sham Hamiltonian. This yields a new  ${}^1D$ , which is used to construct the next  ${}^1H_{KS}[{}^1D]$ . This process is repeated until convergence. It should be noted that  $\tilde{w}$  only needs to be calculated once, and scales as  $\mathcal{O}(N^4)$  due to its dependence on the 2-electron integrals. In practice, the calculation of  $\tilde{w}$  is fast, with the main bottleneck for the DFA 1-RDMFT procedure being the iterative solving of Equation 7. We implement the above minimization for  ${}^1D$  as a linear Semi-Definite Program (SDP), applying the appropriate N-representability constraints such that the resulting  ${}^1D$  is N-representable[67].

As can be seen from the quadratic form of the 1-RDM functional, the 1-RDMFT correction to the energy is only non-zero when idempotency in the 1-RDM ( ${}^1D^2 = {}^1D$ ) is broken. This allows the DFA 1-RDMFT to reproduce traditional KS-DFT results in the absence of strong correlation, where the 1-RDM is idempotent. Consequently, the DFA 1-RDMFT framework retains the accuracy and scaling of traditional KS XC functionals in weakly correlated systems, while compensating static correlation errors in the presence of multi-reference correlation.

### III. COMPUTATIONAL METHODOLOGY

All DFA 1-RDMFT calculations were performed in a spin restricted framework using in-house developed code, which utilizes PySCF[68] for the integral generation, LibXC[69] to evaluate the XC functionals, and CVXPY[70] with the SCS[71] solver for the SDP.[72] An example comparing the timings of DFA 1-RDMFT against UKS DFT, both utilizing the PBE functional from PySCF, along with a discussion of the results, are available in the SI as Table S3 and Figure S4. UKS DFT calculations were performed using ORCA 6.0.0[73] in combination with LibXC. Reference results were obtained with the Anti-Hermitian Contracted Schrodinger Equation (ACSE).[74–77] The cc-pVDZ basis set was utilized for all calculations.[78]

### IV. RESULTS

In this work, we consider the dissociations of  $\text{C}_2$ ,  $\text{N}_2$ ,  $\text{CN}$ ,  $\text{F}_2$ ,  $\text{NO}$ ,  $\text{S}_2$ ,  $\text{SiO}$ , and  $\text{CO}$ . The set of investigated functionals presents a subset of those available in the LibXC library. It includes only full XC functionals, which were denoted with “\_XC\_” in their name or separate exchange “\_X\_” and correlation “\_C\_” components with identical names, which were combined to create the full XC functional. This yields 217 distinct functionals. After removing functionals that failed to converge for any point in any of the systems for 1-RDMFT or DFT, this yields a final set comprising 190 functionals. The functionals used can be broken down into 6 LDAs, 50 GGAs, 15 mGGAs, 78 Hybrids, and 41 RSHs. To ensure that we are comparing differences in the functionals themselves, we equalize the effect of the 1-RDM term across the test set by optimizing the scalar  $\tilde{w}$  value in DFA 1-RDMFT for each system/functional combination individually to reproduce the dissociation energy as obtained from the ACSE. The optimized  $\tilde{w}$  value is then held fixed throughout all internuclear distances for each system/functional combination to generate the dissociation curves from equilibrium to 3 Å for both DFA 1-RDMFT and UKS-DFT. This ensures that we obtain the optimal performance for each XC functional in DFA 1-RDMFT, enabling us to identify trends across Jacob’s ladder and  $\kappa$ . Importantly, this enables us to explore the interplay between the DFA utilized and the 1-RDM corrective term to infer how well correlation is being captured along the entirety of the dissociation curve.

An example of these dissociations ( $\text{N}_2$ ) is presented in Figure 1. To place this work within the broader realm of available techniques, Figure 1 also includes the double hybrid B2-PLYP[79, 80] in both the spin restricted and unrestricted formalisms, as well as MC-PDFT with the translated tPBE and tTPSSH functionals[81, 82]. B2-PLYP, in the restricted KS framework gives excellent performance compared to the reference ACSE curve around equilibrium but breaks down as the bond is stretched. B2-PLYP in the unrestricted KS framework yields a better dissociation limit but displays significant deviations from the ACSE curve in the stretched bond region. MC-PDFT tPBE improves upon UKS PBE, however, MC-PDFT tTPSSH yields larger errors than UKS TPSSH. UKS DFT with both PBE and TPSSH overestimates the dissociated limit. Around the equilibrium geometry, UKS PBE recovers the ACSE potential energy surface whereas UKS TPSSH shows deviations from the ACSE throughout its entirety. Transitioning to DFA 1-RDMFT not only reproduces the dissociated limit, which is the target utilized to determine  $\kappa$ , but also improves upon UKS DFT in the stretched bond region. In the absence of multireference effects (up to  $R(\text{N-N}) = 1.4 \text{ Å}$ ), DFA 1-RDMFT recovers UKS DFT as the 1-RDM remains idempotent.

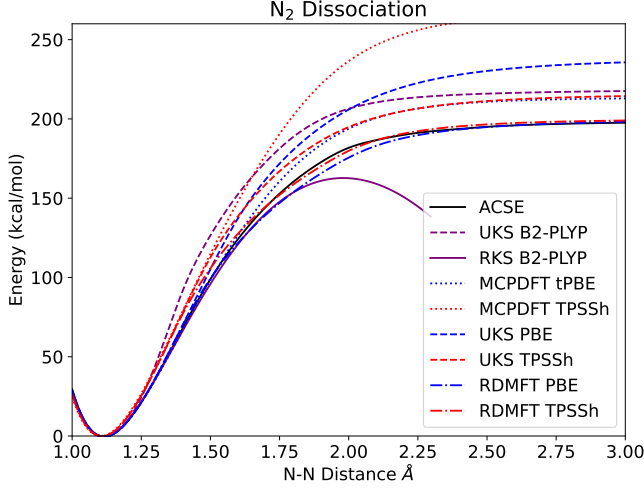


FIG. 1:  $N_2$  dissociation curves comparing the DFA 1-RDMFT, UKS DFT, MCPDFT, and ACSE.

Zeroing all curves using their equilibrium values to facilitate comparisons between functionals and the ACSE, we calculated two error metrics: the maximal error between either the DFA 1-RDMFT or DFT curve and the reference ACSE curve

$$M_e = \max |E_{ACSE}(r) - E_{RDMFT}(r)|, \quad (8)$$

and the cumulative error between the two curves

$$C_a = \int_{eq}^{3\text{\AA}} |E_{ACSE}(r) - E_{RDMFT}(r)| dr. \quad (9)$$

To quantify the maximal error and cumulative error metrics, we compare their averages across all systems for each functional in Figure 2. We observe a nearly linear relationship between the two error metrics, indicating that either is equally valid for the remainder of this work. This also implies that the errors are not localized to a single point along the dissociation but are distributed along it. Plotting the linear regression and  $R^2$  values, we find that, while both show  $R^2$ 's  $> 0.95$ , DFA 1-RDMFT is more linear with a  $R^2$  of 0.997 vs. UKS-DFT's 0.973. This is likely due to DFA 1-RDMFT being able to capture the dissociated limit for all systems whereas DFT, even with spin-symmetry breaking, is unable to achieve this for all systems. Additionally, the slope for UKS-DFT's errors is greater than DFA 1-RDMFT's, 1.196 vs 1.114, indicating the max error is increasing faster than the cumulative error. Again, this is likely due to UKS-DFT not capturing the dissociated limit in all systems. For the remainder of this work, we will utilize the cumulative error as our key metric in the text; max error data may be found in the supplemental information (SI).

In Figure 3 we sort the functionals according to their cumulative error and classify them according to their

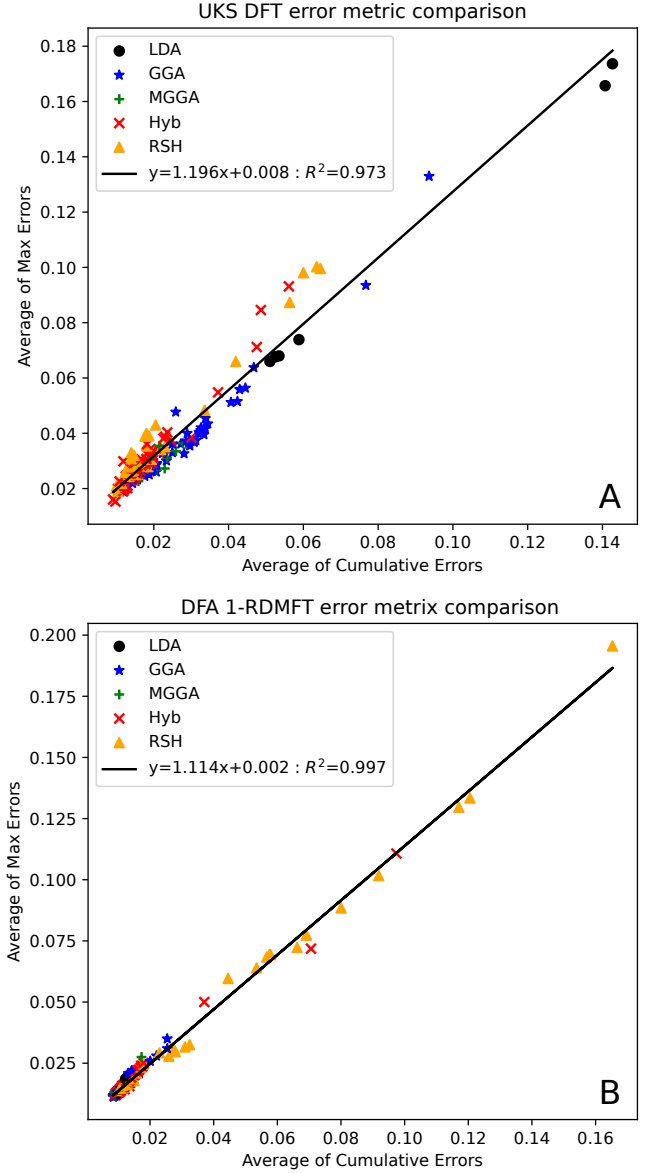


FIG. 2: Plots of the average of max errors vs the average of cumulative errors, in Hartree, for (A): UKS-DFT, and (B): DFA 1-RDMFT results for all systems and functionals used in this work.

placement on Jacob's ladder. The functionals ranks are tabulated and available in Table S2 of the SI. Starting with UKS-DFT, we notice that the best performing functionals are primarily of Hybrid and RSH nature, with mGGA functionals being interspersed throughout. The worst performing functionals are dominated by the GGA and LDA functionals. In contrast, within DFA 1-RDMFT, the functional ordering is largely reversed, with the worst performing functionals comprising mainly Hybrid and RSH functionals, while GGAs and MGGA's yield the best performance. LDA based functionals are interspersed throughout. The cumulative errors

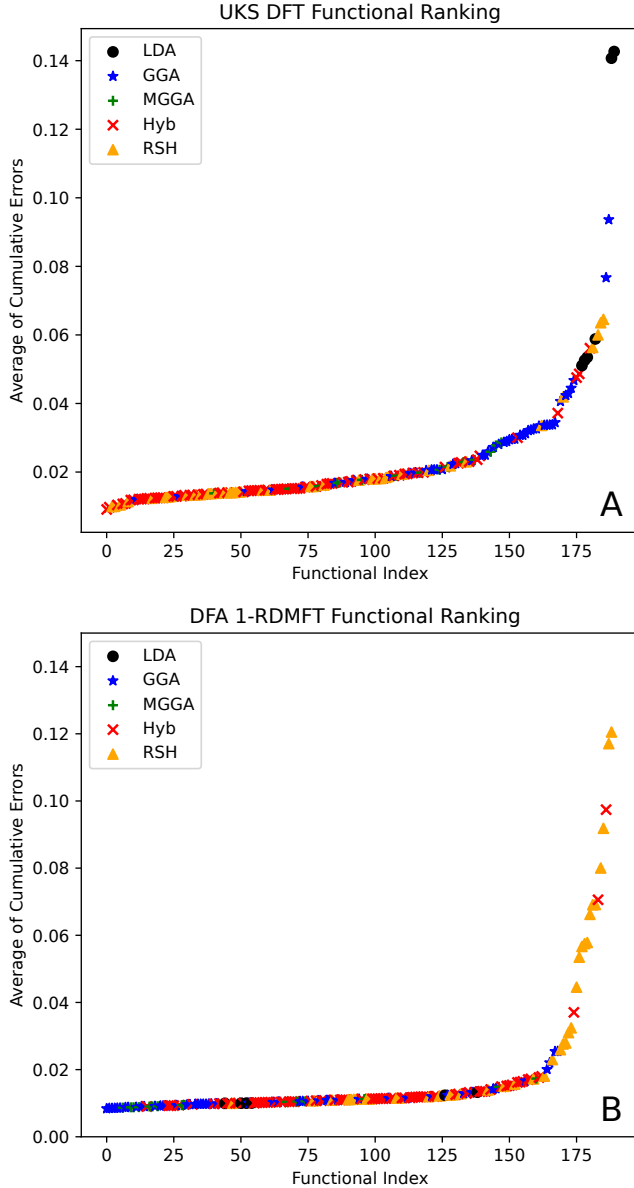


FIG. 3: Plots the functional rankings for (A): UKS-DFT, and (B): DFA 1-RDMFT. The functionals are ranked in order of increasing average of cumulative errors in Hartree.

for UKS-DFT show a greater slope than those for DFA 1-RDMFT, indicating a greater XC functional dependence in UKS-DFT compared to DFA 1-RDMFT, where this dependence is dampened. Analysis of the max errors yields identical conclusions and is presented in the SI (Figure S1).

Comparison of cumulative functional errors between UKS-DFT and DFA 1-RDMFT, as shown in Figure 4, reveals that there is no significant correlation between them. Local functionals span a wide range of errors in UKS DFT but that spread decreases notably when

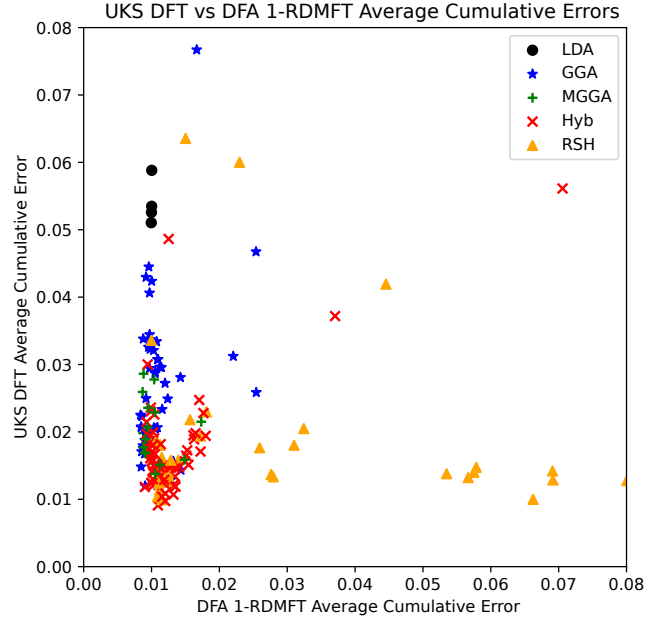


FIG. 4: Comparison of the average cumulative errors, in Hartree, from UKS-DFT and DFA 1-RDMFT for the majority of functionals investigated in this work. Three and four functionals from UKS-DFT and DFA 1-RDMFT, respectively, with errors  $> 0.08$ , are omitted from the figure to improve readability.

moving from LDAs to GGAs and ultimately mGGAs. This is further emphasized by the standard deviations of UKS DFT errors, which are presented in Table II, and are 0.0454, 0.0144, and 0.0046 for LDAs, GGAs, and mGGAs, respectively. Although the local functionals display a wide range of errors in UKS DFT, in DFA 1-RDMFT their error spread is reduced with standard deviations of 0.0015, 0.0040, and 0.0025 for LDAs, GGAs, and mGGAs, respectively. Including exact exchange with hybrid functionals yields standard deviations of 0.0081 and 0.0121 for UKS DFT and DFA 1-RDMFT, respectively, presenting a departure from the behavior of pure functionals, where DFA 1-RDMFT outperforms UKS-DFT. The effects of exact exchange on the DFA 1-RDMFT framework is explored in more detail in the later part of this study. These results indicate that performance of an XC functional in UKS-DFT holds limited predictive power for its performance in DFA 1-RDMFT. Importantly, this emphasizes that UKS-DFT and DFA 1-RDMFT are fundamentally different in the ways they capture correlation, through the XC functional and the breaking of spin-symmetry in UKS-DFT, and through fractional occupations in the 1-RDM and an electron integral derived term in DFA 1-RDMFT. The max errors, available in the SI (Figure S2), again display an identical trend.

Using the Jacob's ladder classification scheme, we

Rung	UKS DFT		DFA 1-RDMFT		$\kappa$
	Func	Error	Func	Error	
LDA	teter93	0.0510	teter93	0.0100	0.1118
GGA	n12	0.0120	hcth_p14	0.0084	0.1048
mGGA	mn15	0.0138	tm	0.0087	0.1029
Hyb	bllyp	0.0091	tpssh	0.0090	0.1347
RSH	camh-b3lyp	0.0100	tuned-cam-b3lyp	0.0100	0.2081

TABLE I: Functionals with the lowest cumulative error, in Hartree, per rung of Jacob’s ladder as obtained with UKS DFT and DFA 1-RDMFT and their associated cumulative error. DFA 1-RDMFTs optimal  $\kappa$  values are also included.

compare the functionals with the lowest cumulative error per rung in Table I along with the DFA 1-RDMFT optimized  $\kappa$  values. LDA presents the only rung for which the lowest errors for both UKS-DFT and DFA 1-RDMFT are achieved with the same functional (Teter93). This is likely due to the limited number of LDAs available (six) in comparison to other rungs. Here, a direct comparison shows that the Teter93 functional performs significantly better when used within 1-RDMFT compared to UKS-DFT. Indeed, comparing the best performing functional on each rung between UKS-DFT and DFA 1-RDMFT reveals that DFA 1-RDMFT always displays a lower cumulative error except for when using a RSH functional, where they display identical errors. The range of errors within DFA 1-RDMFT is notably lower than in UKS-DFT at 0.0016 Hartree vs 0.0419 Hartree, respectively. Interestingly, while UKS-DFT tends to decrease in cumulative error as one ascends Jacob’s ladder, the opposite is found for DFA 1-RDMFT. Inspection of the performance of commonly utilized, popular functionals reveals TPSSH and N12 as good candidates for common use cases, where, for example, geometries are optimized at the DFT level while further electronic properties are obtained from subsequent DFA 1-RDMFT single point calculations. It should be noted that DFA 1-RDMFT includes the UKS DFT error around equilibrium as in weakly correlated regions where no breaking of spin symmetry occurs in UKS DFT DFA 1-RDMFT reproduces the DFT energies.

To further explore the effect of the XC functional form on the accuracy of UKS-DFT and DFA 1-RDMFT calculations, we investigate the average cumulative errors and their standard deviations per rung of Jacob’s ladder (Table II). This analysis reveals that DFA 1-RDMFT’s errors generally are significantly lower than those obtained from UKS-DFT. Again, the only rung that presents an exception to this trend is the RSHs, where 1-RDMFT performs worse than UKS-DFT. Critically, within DFA 1-RDMFT, no large differences between the local functionals (LDA, GGA, and MGGA) are observed, but errors increase significantly when introducing hybrid and especially RSH functionals. In

Rung	UKS DFT		DFA 1-RDMFT	
	Error	Stdev	Error	Stdev
LDA	0.0832	0.0454	0.0109	0.0015
GGA	0.0291	0.0144	0.0113	0.0040
mGGA	0.0204	0.0046	0.0104	0.0025
Hyb	0.0173	0.0081	0.0140	0.0121
RSH	0.0207	0.0147	0.0364	0.0364

TABLE II: The average cumulative errors and standard deviations, in Hartree, for each rung of Jacob’s ladder for both UKS DFT and DFA 1-RDMFT.

contrast, the best performing rung for UKS-DFT is hybrid functionals. Comparison of standard deviations identifies that DFA 1-RDMFT significantly reduces the differences in the errors for the local functionals with respect to UKS-DFT, while increasing the deviations for the Hybrid and RSH functionals. We believe the improvement in the performance of local functionals with DFA 1-RDMFT may primarily be due to a more accurate representation of the underlying electron density introduced by fractional orbital occupations, as was argued in previous work that allowed fractional occupations without the 1-RDM energetic correction[83]. The increase in errors in hybrid functionals is thought to derive from the 1-RDM corrective term’s dependence on HF exchange and the use of a spin-restricted 1-RDM (*vide infra*).

Since the DFA 1-RDMFT energy is dependent on both the XC and 1-RDM functionals, the varying  $\kappa$  values indicate the balance struck between correlation effects captured via the XC functional and those captured by the 1-RDM functional, with a larger value of  $\kappa$  denoting a stronger 1-RDM correction. As  $\tilde{w} = \frac{\kappa \text{Tr}(^2I)}{\text{Tr}(^2W^2I)} \sum_{ij} (2\langle \tilde{i}j | \tilde{i}j \rangle - \langle \tilde{i}j | j\tilde{i} \rangle)$  is derived from the electron repulsion integrals, and was optimized for each system/functional combination separately, we can use this to calculate the optimal  $\kappa$  value for each functional. The results of this analysis are plotted in Figure 5. We again find that functionals of the same rung tend to cluster together with similar  $\kappa$  values. As is evident from the figure, GGAs and mGGAs require the smallest  $\kappa$  values and thus the least correction from the 1-RDM term, whereas hybrid and RSH functionals both require significantly stronger corrections.

To determine whether there is a relationship between the optimal  $\kappa$  values and the cumulative errors, we plot both for DFA 1-RDMFT and UKS-DFT in Figure 6. We include UKS-DFT here as, although UKS-DFT does not have a dependence on  $\kappa$ , it may correlate with the XC functional’s inherent ability to capture strong correlation in the spin-symmetry broken regime. We find that in UKS-DFT, GGAs, while constrained to only a small range of optimal  $\kappa$  values, display high variability in the

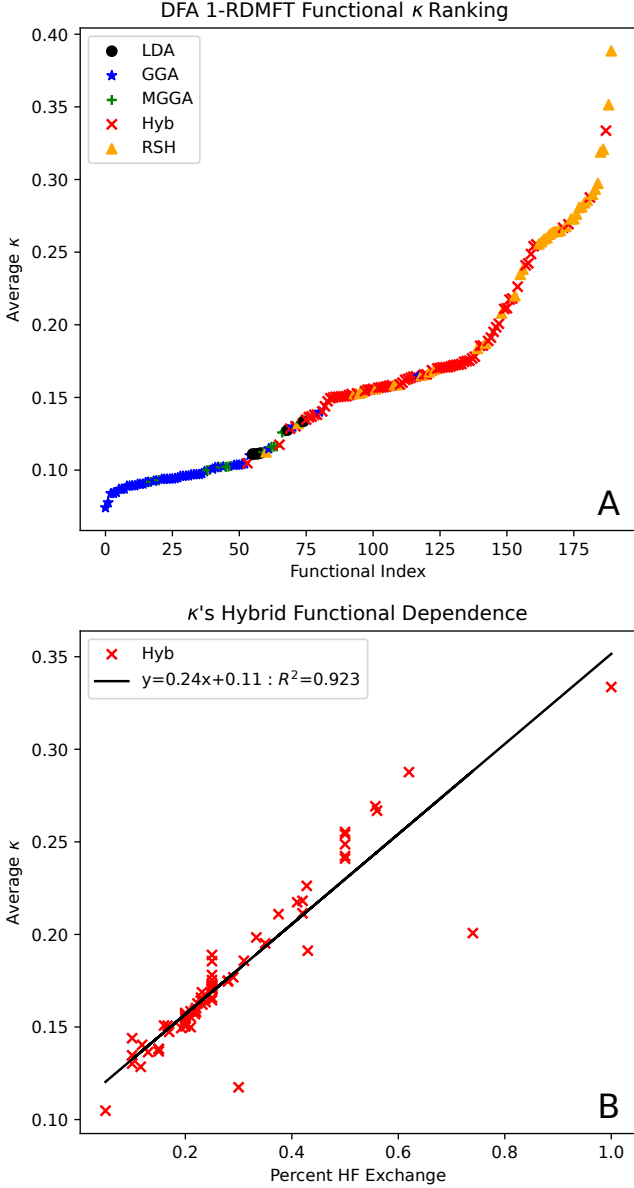


FIG. 5: (A): Plot of the functional ranking according to the optimal average  $\kappa$  value, and (B): a plot of the relationship between HF exchange and the  $\kappa$  value.

corresponding error. Hybrids, on the contrary, span a wider range of  $\kappa$  values but show a tighter grouping in terms of error. As there is no clear trend between the  $\kappa$  value and the resulting cumulative error, this implies that  $\kappa$  does not relate to an XC functional's ability to capture strong correlation in UKS-DFT. In DFA 1-RDMFT,  $\kappa$  values for LDAs, GGAs, and MGGA are closely clustered together in the 0.05 to 0.10 range. The observed minimum in the errors suggests that a  $\kappa$  value of approximately 0.075 yields the lowest errors with traditional XC functionals in DFA 1-RDMFT. This implies that there is an optimal value of  $\kappa$  such that each functional, XC and 1-RDM, contribute, in a

balanced manner, to the overall description of electron correlation. As the 1-RDM correction is zero in the weakly correlated regime, the XC functional and  $\kappa$  must facilitate a smooth transition in the capture of electron correlation as the 1-RDM term becomes increasingly active to minimize the overall error. Hybrid functionals do not display a clear  $\kappa$  minimum, instead showing a clearer relationship between cumulative errors and  $\kappa$ . Plotting the percent HF exchange for the functional vs its cumulative error (available in the SI, Figure S3) reproduces this trend, with the smallest errors occurring for functionals with HF exchange  $< 20\%$ . For both UKS-DFT and DFA 1-RDMFT, RSHs results show no discernible trends.

Plotting the Hybrid functionals according to their percent HF exchange reveals a notable trend between the optimal  $\kappa$  value and the amount of HF exchange included in the XC functional (Figure 5). An  $R^2$  value of 0.923 implies that  $\kappa$  has a near linear dependence on the underlying amount of HF exchange in a given functional. Equation 7 gives insight into why this is the case;  $\tilde{w}$  is part of the corrective 1-RDM term, which has a dependence on the exchange integrals. Since  ${}^1D^2 - {}^1D$  is always non-positive, the 1-RDM correction acts against the increase in the exchange contribution. Therefore, increasing the amount of exchange in a functional implies a larger correction, with  $\kappa$  or  $\tilde{w}$  increasing.

To identify if this relationship extends to the errors in DFA 1-RDMFT, we plot the Hybrid functionals' percent HF exchange against the average of cumulative errors in Figure 7 for both UKS DFT and DFA 1-RDMFT. Although HF exchange increases static correlation errors in DFT,[84–86] this issue can be masked by the breaking of spin symmetry.[87] As a result, no significant dependence of the cumulative errors on the amount of HF exchange used within UKS DFT is observed. In contrast, in DFA 1-RDMFT, there is a strong relationship between the cumulative error and the amount of HF exchange. The cumulative error is minimized with  $\approx 10\%$  HF exchange. Increases in the HF exchange fraction beyond this point result in larger cumulative errors until approaching an asymptotic limit. This difference in behavior from UKS DFT is likely caused by a combination of two factors: the use of a spin-restricted framework within DFA 1-RDMFT, and the underlying dependence of the 1-RDM correction term on the exchange integrals.

To further elucidate the dependence on HF exchange, we selected four different XC functionals (PBE, TPSS, SCAN, and B3LYP) and varied the fraction of HF exchange according to:

$$E_x = (1 - \lambda)F_X + \lambda HF_X, \quad (10)$$

where  $F_X$  is the XC functional's non-HF exchange and  $HF_X$  is HF exchange. We varied  $\lambda$  from 0 to 1 in increments of 0.05 for each functional and re-optimized

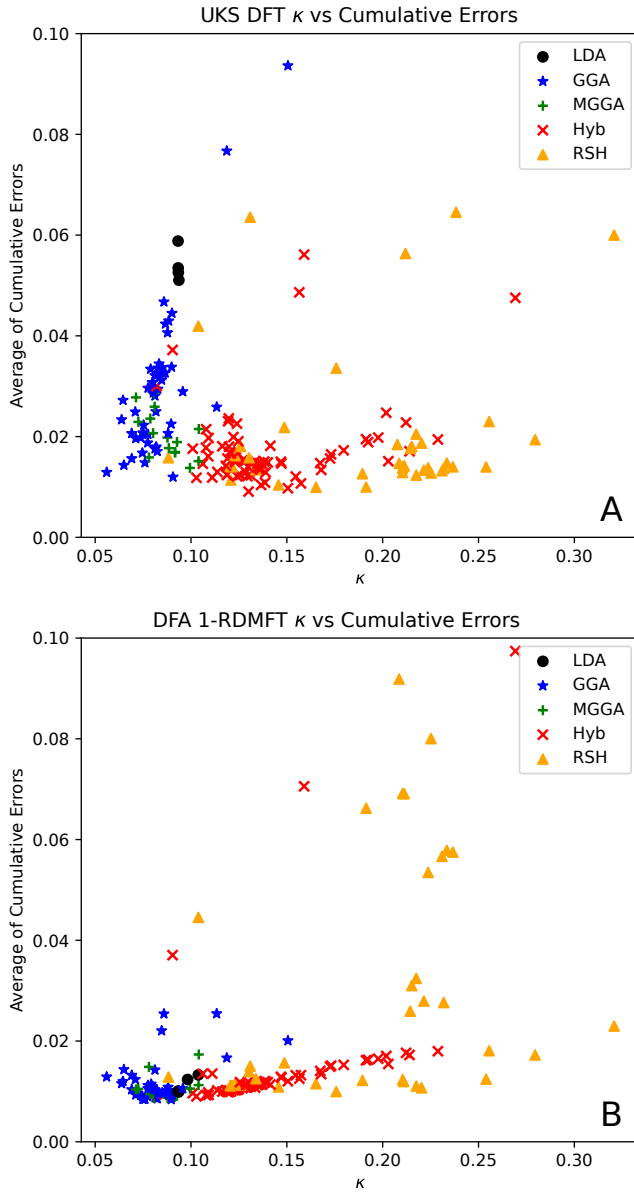


FIG. 6: Plots of the cumulative error in Hartree vs  $\kappa$  for (A): UKS-DFT and (B): DFA 1-RDMFT. Two and three functionals with errors  $> 0.1$  in UKS-DFT and DFA 1-RDMFT, respectively, are omitted from the figure to improve readability.

$\tilde{w}$ , allowing the quantification of its dependence on the HF exchange fraction included in the XC functional. Multiple functionals with different base correlation and exchange components were used to identify how their differences contribute to  $\kappa$ .

Examples of the regressions obtained are displayed in Figure 8. The results shown for  $C_2$  are representative of all other systems; the relationship between HF exchange and the optimal  $\tilde{w}$  value is linear, with a  $R^2$  value greater than 0.999 for all system. Comparing the slopes between

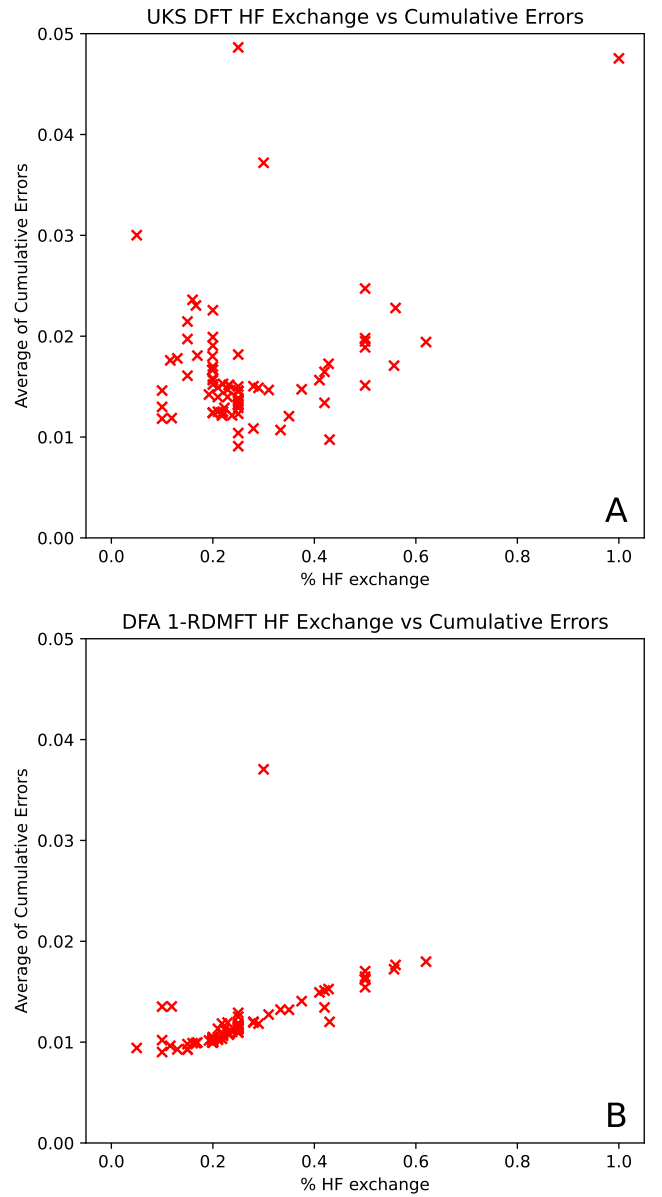


FIG. 7: Plots of the cumulative error in Hartree vs HF exchange for (A): UKS-DFT and (B): DFA 1-RDMFT. One and two functionals with errors  $> 0.05$  in UKS-DFT and DFA 1-RDMFT, respectively, are omitted from the figure to improve readability.

the systems (shown in Table III), we note that the slopes for B3LYP, TPSS, and PBE are nearly identical when applied to the same system. SCAN presents the only outlier, with its slope consistently  $\approx 0.02$  lower than the other functionals.

The aforementioned scans included the point  $\lambda = 1$ , where each functional contains only HF exchange. At this point, the only difference between functionals arises from their correlation terms. The fact that the  $\tilde{w}$  values at this point are not identical confirms that  $\tilde{w}$  depends



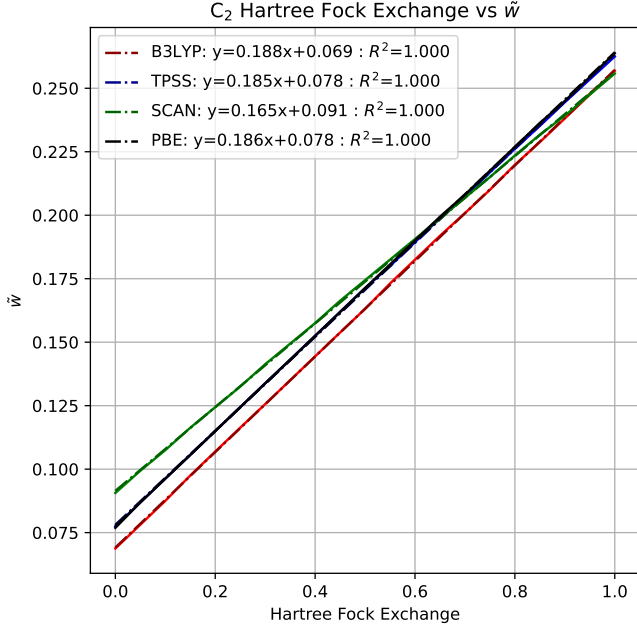


FIG. 8: Plot of functional HF exchange vs optimal  $\tilde{w}$  value for C<sub>2</sub>. Linear regressions are also plotted and nearly perfectly cover the underlying data. TPSS and PBE data lie effectively on top of each other.

System	Functional			
	B3LYP	PBE	SCAN	TPSS
C <sub>2</sub>	0.188	0.186	0.165	0.185
CN	0.220	0.218	0.197	0.216
CO	0.246	0.246	0.223	0.242
F <sub>2</sub>	0.315	0.316	0.294	0.309
N <sub>2</sub>	0.246	0.246	0.224	0.243
NO	0.259	0.259	0.237	0.256
S <sub>2</sub>	0.159	0.158	0.145	0.156
SiO	0.201	0.202	0.182	0.197

TABLE III: Slope of the linear regression between the optimal value of  $\tilde{w}$  and HF exchange. All  $R^2$  values are greater than 0.999.

on the correlation term in the underlying XC functional. This is the result of the interplay between the XC and 1-RDM functionals. Different XC functionals will capture varying fractions of the correlation to be described by the 1-RDM functional[88]. To further investigate this, we compare the  $\lambda = 1$  point for all functionals (available in the SI (Table S1)), which reveals that different correlation terms only result in small differences in the  $\tilde{w}$  value, on the order of  $\approx 0.01$ . These results imply that the overlapping correlation obtained by both the XC and 1-RDM functional is relatively minor. In contrast, changing the system while utilizing the same XC functional, results in significantly larger changes to  $\tilde{w}$  of up to  $\approx 0.1$ .

To further elucidate the dependence of  $\tilde{w}$  on HF

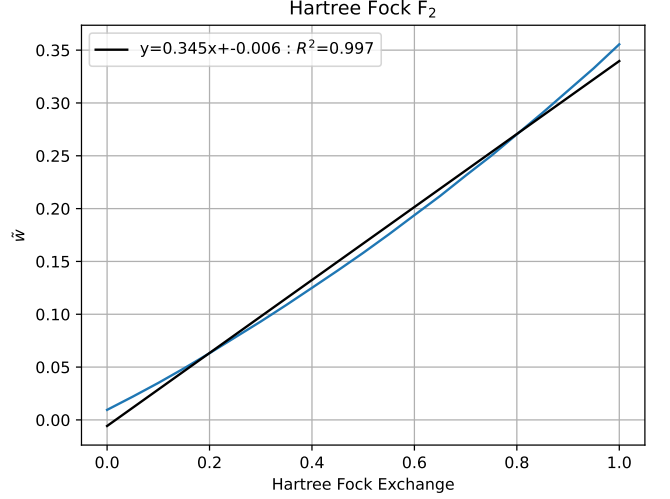


FIG. 9: Plot of the fraction of HF exchange in DFA 1-RDMFT utilizing the HF XC functional vs the optimal  $\tilde{w}$  value for F<sub>2</sub>. The linear regression is also plotted to emphasize the slight but notable non-linear behavior.

exchange, we linearly interpolate between Hartree and Hartree-Fock theory by modulating the amount of exchange in DFA 1-RDMFT using the HF functional. As shown in Figure 9 for F<sub>2</sub>, we now observe a slight curvature in the relationship between  $\tilde{w}$  and HF exchange. This implies that the previously observed linear behavior in XC functionals is due to the interplay between the functional's exchange term and HF exchange with both being slightly non-linear on their own. In the 1-RDM term  $\tilde{w}\text{Tr}({}^1D^2 - {}^1D)$  in DFA 1-RDMFT,  $\tilde{w}$  has a linear dependence on the exchange integrals; however,  ${}^1D^2 - {}^1D$  is non-linear. This is likely the origin for the non-linear relationship between  $\tilde{w}$  and HF exchange.

## V. CONCLUSION

In this paper, we explored how the accuracy of the previously developed DFA 1-RDMFT, a method which combines a 1-RDM functional with existing XC functionals, depends on the utilized XC functional and we compare the results to the traditional UKS-DFT approach. In this DFA 1-RDMFT framework, the role of the 1-RDM term is to capture strong electron correlation effects, while the XC functional captures the remaining (dynamic) correlation effects. The balance between the two terms is tuned via the functional dependent parameter  $\kappa$ . The DFA 1-RDMFT framework needs to smoothly transition between XC-only regimes in the absence of strong correlation, where the KS-DFT result is recovered, and those where the 1-RDM term is non-zero. An XC functional that already yields good

results in strongly correlated systems may produce poor results when used in DFA 1-RDMFT due to overlapping contributions to the energy.

Systematically benchmarking 190 functionals available in the LibXC library, we find that functionals on the same rung of Jacob’s ladder generally yield comparable performance within either UKS-DFT or DFA 1-RDMFT. However, the trend of functionals generally increasing in accuracy as one ascends Jacob’s ladder, which is observed in UKS-DFT, is reversed in DFA 1-RDMFT, where GGAs and MGGA’s outperformed Hybrid and RSH functionals. Importantly, DFA 1-RDMFT yields lower average cumulative errors for every rung of Jacob’s ladder except for RSHs, while displaying significantly less dependence on the underlying XC functional as compared to UKS-DFT. In general, we note that DFA 1-RDMFT displays better convergence behavior, lower overall errors, and less functional dependence than UKS-DFT.

Investigating the performance of Hybrid XC functionals in DFA 1-RDMFT, we also reveal a linear dependence of DFA 1-RDMFT’s  $\tilde{w}$  value on the fraction of HF exchange in XC functionals, with a higher HF exchange fraction necessitating a larger  $\tilde{w}$  value. While  $\tilde{w}$  has a dependence on the exchange integrals, by utilizing this exchange relationship through Hartree and Hartree-Fock theory, we find that the linearity arises from a cancellation of non-linear dependencies in the XC functional’s exchange term and HF exchange on  $\tilde{w}$ .

Furthermore, we also obtained the  $\kappa$  values necessary to utilize the vast majority of functionals available in LibXC within DFA 1-RDMFT, significantly expanding its utility. These values are tabulated in the SI (Table S2). We find that a low  $\kappa$  value does not necessarily yield high accuracy. Instead, we find that functionals with  $\kappa \approx 0.075$  yield the lowest errors, implying that a careful balance between electron correlation recovered through the XC functional and the 1-RDM functional is required to ensure a complete description of electron correlation effects in the presence of strong correlation. The lack of a clear relationship between the DFA 1-RDMFT  $\kappa$  value for a given XC functional and its accuracy in UKS-DFT, implies that DFA 1-RDMFT and UKS-DFT capture strong correlation effects through fundamentally different mechanisms.

Further efforts are currently underway to verify the transferability of the insights gained in this work, including utilizing a subset of the functionals demonstrated to provide high accuracy, to investigate the properties and reactivity of larger, more complex strongly correlated systems of chemical interest. We believe that the overall trends and insights found throughout this work are transferable beyond diatomics. For the systems considered in this work, our data suggests that TPSSh

and N12 present widely available XC functionals with good accuracy in both DFT and DFA 1-RDMFT across both single-reference and strongly correlated regimes.

## ACKNOWLEDGMENTS

Daniel Gibney thanks Samuel Warren for insightful discussions regarding the HF exchange term. The authors thank the University of Minnesota for startup funding.

## SUPPORTING INFORMATION

The Supplemental Material contains the max error figures, the optimal  $\tilde{w}$  values for 100% HF exchange SCAN, B3LYP, TPSS, and PBE, plots of cumulative error vs  $\kappa$ , and the tabulated  $\kappa$ , average max and cumulative error values and timing data for N<sub>2</sub>.

- 
- [1] Kohn, W.; Sham, L. J. Self-Consistent Equations Including Exchange and Correlation Effects. *Phys. Rev.* **1965**, *140*, A1133–A1138.
- [2] Hohenberg, P.; Kohn, W. Inhomogeneous Electron Gas. *Phys. Rev.* **1964**, *136*, B864–B871.
- [3] Dumaz, M.; Boucher, R.; Marques, M. A. L.; Romero, A. H. Authorship and citation cultural nature in Density Functional Theory from solid state computational packages. *Scientometrics* **2021**, *126*, 6681–6695.
- [4] Burke, K. Perspective on density functional theory. *J. Chem. Phys.* **2012**, *136*, 150901.
- [5] Parr, R. G. Density Functional Theory of Atoms and Molecules. Horizons of Quantum Chemistry. Dordrecht, 1980; pp 5–15.
- [6] Kohanoff, J. *Electronic Structure Calculations for Solids and Molecules: Theory and Computational Methods*; Cambridge University Press, 2006.
- [7] Patchkovskii, S.; Ziegler, T. Improving “difficult” reaction barriers with self-interaction corrected density functional theory. *J. Chem. Phys.* **2002**, *116*, 7806–7813.
- [8] Scott, A. P.; Radom, L. Harmonic Vibrational Frequencies: An Evaluation of Hartree-Fock, Møller-Plesset, Quadratic Configuration Interaction, Density Functional Theory, and Semiempirical Scale Factors. *J. Phys. Chem.* **1996**, *100*, 16502–16513.
- [9] Laurent, A. D.; Jacquemin, D. TD-DFT benchmarks: A review. *Int. J. Quantum Chem.* **2013**, *113*, 2019–2039.
- [10] Zhan, C.-G.; Nichols, J. A.; Dixon, D. A. Ionization Potential, Electron Affinity, Electronegativity, Hardness, and Electron Excitation Energy: Molecular Properties from Density Functional Theory Orbital Energies. *J. Phys. Chem. A* **2003**, *107*, 4184–4195.
- [11] Karton, A.; Spackman, P. R. Evaluation of density functional theory for a large and diverse set of organic and inorganic equilibrium structures. *J. Comput. Chem.* **2021**, *42*, 1590–1601.
- [12] Mardirossian, N.; Head-Gordon, M. Thirty years of density functional theory in computational chemistry: an overview and extensive assessment of 200 density functionals. *Molecular Physics* **2017**, *115*, 2315–2372.
- [13] Cohen, A. J.; Mori-Sánchez, P.; Yang, W. Insights into Current Limitations of Density Functional Theory. *Science* **2008**, *321*, 792–794.
- [14] Polo, V.; Kraka, E.; Cremer, D. Electron correlation and the self-interaction error of density functional theory. *Mol. Phys.* **2002**, *100*, 1771–1790.
- [15] Cohen, A. J.; Mori-Sánchez, P.; Yang, W. Challenges for density functional theory. *Chem. Rev.* **2012**, *112*, 289–320.
- [16] Perdew, J. P.; Schmidt, K. Jacob’s ladder of density functional approximations for the exchange-correlation energy. *AIP Conf. Proc.* **2001**, *577*, 1–20.
- [17] Møller, C.; Plesset, M. S. Note on an Approximation Treatment for Many-Electron Systems. *Phys. Rev.* **1934**, *46*, 618–622.
- [18] Görling, A.; Levy, M. Exact Kohn-Sham scheme based on perturbation theory. *Phys. Rev. A* **1994**, *50*, 196–204.
- [19] Su, N. Q.; Xu, X. Development of New Density Functional Approximations. *Annual Review of Physical Chemistry* **2017**, *68*, 155–182.
- [20] Yu, H. S.; He, X.; Truhlar, D. G. *J. Chem. Theory Comput.* **2016**, *12*, 1280–1293.
- [21] Zhao, Y.; Truhlar, D. G. A new local density functional for main-group thermochemistry, transition metal bonding, thermochemical kinetics, and noncovalent interactions. *The Journal of chemical physics* **2006**, *125*.
- [22] Peverati, R.; Truhlar, D. G. M11-L: A local density functional that provides improved accuracy for electronic structure calculations in chemistry and physics. *The Journal of Physical Chemistry Letters* **2012**, *3*, 117–124.
- [23] Peverati, R.; Truhlar, D. G. An improved and broadly accurate local approximation to the exchange–correlation density functional: The MN12-L functional for electronic structure calculations in chemistry and physics. *Physical Chemistry Chemical Physics* **2012**, *14*, 13171–13174.
- [24] Medvedev, M. G.; Bushmarinov, I. S.; Sun, J.; Perdew, J. P.; Lyssenko, K. A. Density functional theory is straying from the path toward the exact functional. *Science* **2017**, *355*, 49–52.
- [25] Brorsen, K. R.; Yang, Y.; Pak, M. V.; Hammes-Schiffer, S. Is the Accuracy of Density Functional Theory for Atomization Energies and Densities in Bonding Regions Correlated? *The Journal of Physical Chemistry Letters* **2017**, *8*, 2076–2081, PMID: 28421759.
- [26] Tao, J.; Perdew, J. P.; Staroverov, V. N.; Scuseria, G. E. Climbing the Density Functional Ladder: Nonempirical Meta-Generalized Gradient Approximation Designed for Molecules and Solids. *Phys. Rev. Lett.* **2003**, *91*, 146401.
- [27] Perdew, J. P.; Ruzsinszky, A.; Csonka, G. I.; Constantin, L. A.; Sun, J. Workhorse Semilocal Density Functional for Condensed Matter Physics and Quantum Chemistry. *Phys. Rev. Lett.* **2009**, *103*, 026403.
- [28] Sun, J.; Ruzsinszky, A.; Perdew, J. P. Strongly Constrained and Appropriately Normed Semilocal Density Functional. *Phys. Rev. Lett.* **2015**, *115*, 036402.
- [29] Becke, A. D. Density functionals for static, dynamical, and strong correlation. *The Journal of Chemical Physics* **2013**, *138*, 074109.
- [30] Perdew, J. P.; Ruzsinszky, A.; Sun, J.; Nepal, N. K.; Kaplan, A. D. Interpretations of ground-state symmetry breaking and strong correlation in wavefunction and density functional theories. *Proceedings of the National Academy of Sciences* **2021**, *118*, e2017850118.

- [31] Gräfenstein, J.; Kraka, E.; Filatov, M.; Cremer, D. Can Unrestricted Density-Functional Theory Describe Open Shell Singlet Biradicals? *International Journal of Molecular Sciences* **2002**, *3*, 360–394.
- [32] Pople, J. A.; Nesbet, R. K. Self-Consistent Orbitals for Radicals. *The Journal of Chemical Physics* **1954**, *22*, 571–572.
- [33] Berthier, G. Extension de la methode du champ moleculaire self-consistent a l’etude des couches incompletes. *Comptes Rendus Hebdomadaires des Séances de l’Académie des Sciences* **1954**, *238*, 91–93.
- [34] Su, N. Q.; Li, C.; Yang, W. Describing strong correlation with fractional-spin correction in density functional theory. *Proceedings of the National Academy of Sciences* **2018**, *115*, 9678–9683.
- [35] Mahler, A.; Williams, J.; Su, N. Q.; Yang, W. Localized orbital scaling correction for periodic systems. *Phys. Rev. B* **2022**, *106*, 035147.
- [36] Perdew, J. P.; Parr, R. G.; Levy, M.; Balduz, J. L. Density-Functional Theory for Fractional Particle Number: Derivative Discontinuities of the Energy. *Phys. Rev. Lett.* **1982**, *49*, 1691–1694.
- [37] Su, N. Q. Approximate functionals in hypercomplex Kohn–Sham theory. *Electronic Structure* **2022**, *4*, 014011.
- [38] Su, N. Q. Unity of Kohn–Sham density-functional theory and reduced-density-matrix-functional theory. *Phys. Rev. A* **2021**, *104*, 052809.
- [39] Zhang, T.; Su, N. Q. Progress toward a formal functional theory of strongly correlated systems. *Phys. Rev. A* **2023**, *108*, 052801.
- [40] Lee, J.; Bertels, L. W.; Small, D. W.; Head-Gordon, M. Kohn–Sham Density Functional Theory with Complex, Spin-Restricted Orbitals: Accessing a New Class of Densities without the Symmetry Dilemma. *Phys. Rev. Lett.* **2019**, *123*, 113001.
- [41] Gilbert, T. L. Hohenberg–Kohn theorem for nonlocal external potentials. *Phys. Rev. B* **1975**, *12*, 2111–2120.
- [42] Levy, M. Universal variational functionals of electron densities, first-order density matrices, and natural spin-orbitals and solution of the  $v$ -representability problem. *Proc. Natl. Acad. Sci.* **1979**, *76*, 6062–6065.
- [43] Valone, S. M. Consequences of extending 1-matrix energy functionals from pure-state representable to all ensemble representable 1 matrices. *J. Chem. Phys.* **1980**, *73*, 1344–1349.
- [44] Müller, A. Explicit approximate relation between reduced two- and one-particle density matrices. *Phys. Lett. A* **1984**, *105*, 446–452.
- [45] Goedecker, S.; Umrigar, C. J. Natural Orbital Functional for the Many-Electron Problem. *Phys. Rev. Lett.* **1998**, *81*, 866–869.
- [46] Mazziotti, D. A. Geminal functional theory: A synthesis of density and density matrix methods. *J. Chem. Phys.* **2000**, *112*, 10125–10130.
- [47] Piris, M. Reduced-Density-Matrix Mechanics: With Application to Many-Electron Atoms and Molecules. *Adv. Chem. Phys.* **2007**, *134*, 385–427.
- [48] Sharma, S.; Dewhurst, J. K.; Lathiotakis, N. N.; Gross, E. K. U. Reduced density matrix functional for many-electron systems. *Phys. Rev. B* **2008**, *78*, 201103.
- [49] Rohr, D. R.; Pernal, K.; Gritsenko, O. V.; Baerends, E. J. A density matrix functional with occupation number driven treatment of dynamical and nondynamical correlation. *J. Chem. Phys.* **2008**, *129*, 164105.
- [50] Piris, M. Global Method for Electron Correlation. *Phys. Rev. Lett.* **2017**, *119*, 063002.
- [51] Schmidt, J.; Benavides-Riveros, C. L.; Marques, M. A. L. Reduced density matrix functional theory for superconductors. *Phys. Rev. B* **2019**, *99*, 224502.
- [52] Buchholz, F.; Theophilou, I.; Nielsen, S. E. B.; Ruggenthaler, M.; Rubio, A. Reduced Density-Matrix Approach to Strong Matter-Photon Interaction. *ACS Photonics* **2019**, *6*, 2694–2711.
- [53] Pernal, K.; Giesbertz, K. J. H. In *Density-Functional Methods for Excited States*; Ferré, N., Filatov, M., Huix-Rotllant, M., Eds.; Springer International Publishing: Cham, 2016; pp 125–183.
- [54] Piris, M. Global Natural Orbital Functional: Towards the Complete Description of the Electron Correlation. *Phys. Rev. Lett.* **2021**, *127*, 233001.
- [55] Schilling, C.; Schilling, R. Diverging Exchange Force and Form of the Exact Density Matrix Functional. *Phys. Rev. Lett.* **2019**, *122*, 013001.
- [56] Sharma, S.; Dewhurst, J. K.; Shallcross, S.; Gross, E. K. U. Spectral Density and Metal-Insulator Phase Transition in Mott Insulators within Reduced Density Matrix Functional Theory. *Phys. Rev. Lett.* **2013**, *110*, 116403.
- [57] Pernal, K. Turning reduced density matrix theory into a practical tool for studying the Mott transition. *New Journal of Physics* **2015**, *17*, 111001.
- [58] Piris, M. A new approach for the two-electron cumulant in natural orbital functional theory. *Int. J. Quantum Chem.* **2006**, *106*, 1093–1104.
- [59] Piris, M. A natural orbital functional based on an explicit approach of the two-electron cumulant. *Int. J. Quantum Chem.* **2013**, *113*, 620–630.
- [60] Piris, M.; Ugalde, J. M. Perspective on natural orbital functional theory. *Int. J. Quantum Chem.* **2014**, *114*, 1169–1175.
- [61] Pernal, K.; Giesbertz, K. J. H. In *Density-Functional Methods for Excited States*; Ferré, N., Filatov, M., Huix-Rotllant, M., Eds.; Springer International Publishing: Cham, 2016; pp 125–183.
- [62] Gibney, D.; Boyn, J.-N.; Mazziotti, D. A. Density Functional Theory Transformed into a One-Electron Reduced-Density-Matrix Functional Theory for the Capture of Static Correlation. *The Journal of Physical Chemistry Letters* **2022**, *13*, 1382–1388, PMID: 35113577.
- [63] Gibney, D.; Boyn, J.-N.; Mazziotti, D. A. Universal Generalization of Density Functional Theory for Static Correlation. *Phys. Rev. Lett.* **2023**, *131*, 243003.
- [64] Gibney, D.; Boyn, J.-N.; Mazziotti, D. A. Enhancing density-functional theory for static correlation in large molecules. *Phys. Rev. A* **2024**, *110*, L040802.
- [65] Gibney, D.; Boyn, J.-N.; Mazziotti, D. A. Comparison of Density-Matrix Corrections to Density Functional Theory. *Journal of Chemical Theory and Computation* **2022**, *18*, 6600–6607, PMID: 36287002.
- [66] Mazziotti, D. A. Parametrization of the Two-Electron Reduced Density Matrix for its Direct Calculation without the Many-Electron Wave Function. *Phys. Rev. Lett.* **2008**, *101*, 253002.
- [67] Coleman, A. J. Structure of Fermion Density Matrices. *Rev. Mod. Phys.* **1963**, *35*, 668–686.
- [68] Sun, Q.; Berkelbach, T. C.; Blunt, N. S.; Booth, G. H.; Guo, S.; Li, Z.; Liu, J.; McClain, J. D.; Sayfutyarova, E. R.; Sharma, S.; Wouters, S.; Chan, G. K.-

- L. PySCF: the Python-based simulations of chemistry framework. *Wiley Interdiscip. Rev. Comput. Mol. Sci.* **2018**, *8*, e1340.
- [69] Lehtola, S.; Steigemann, C.; Oliveira, M. J.; Marques, M. A. Recent developments in libxc — A comprehensive library of functionals for density functional theory. *SoftwareX* **2018**, *7*, 1–5.
- [70] Diamond, S.; Boyd, S. CVXPY: A Python-embedded modeling language for convex optimization. *J. Mach. Learn. Res.* **2016**, *17*, 1–5.
- [71] O’Donoghue, B.; Chu, E.; Parikh, N.; Boyd, S. SCS: Splitting Conic Solver, version 3.2.4. <https://github.com/cvxgrp/scs>, 2023.
- [72] O’Donoghue, B.; Chu, E.; Parikh, N.; Boyd, S. Conic Optimization via Operator Splitting and Homogeneous Self-Dual Embedding. *J. Optim. Theory Appl.* **2016**, *169*, 1042–1068.
- [73] Neese, F. The ORCA program system. *2*, 73–78, eprint: <https://onlinelibrary.wiley.com/doi/pdf/10.1002/wcms.81>.
- [74] Mazziotti, D. A. Multireference many-electron correlation energies from two-electron reduced density matrices computed by solving the anti-Hermitian contracted Schrödinger equation. *Phys. Rev. A* **2007**, *76*, 052502.
- [75] Mazziotti, D. A. Anti-Hermitian Contracted Schrödinger Equation: Direct Determination of the Two-Electron Reduced Density Matrices of Many-Electron Molecules. *Phys. Rev. Lett.* **2006**, *97*, 143002.
- [76] Mazziotti, D. A. Anti-Hermitian part of the contracted Schrödinger equation for the direct calculation of two-electron reduced density matrices. *Phys. Rev. A* **2007**, *75*, 022505.
- [77] Gidofalvi, G.; Mazziotti, D. A. Spin and symmetry adaptation of the variational two-electron reduced-density-matrix method. *Phys. Rev. A* **2005**, *72*, 052505.
- [78] Dunning, T. H. Gaussian basis sets for use in correlated molecular calculations. I. The atoms boron through neon and hydrogen. *The Journal of Chemical Physics* **1989**, *90*, 1007–1023.
- [79] Grimme, S. Semiempirical hybrid density functional with perturbative second-order correlation. *The Journal of Chemical Physics* **2006**, *124*, 034108.
- [80] Neese, F.; Schwabe, T.; Grimme, S. Analytic derivatives for perturbatively corrected “double hybrid” density functionals: Theory, implementation, and applications. *The Journal of Chemical Physics* **2007**, *126*, 124115.
- [81] Li Manni, G.; Carlson, R. K.; Luo, S.; Ma, D.; Olsen, J.; Truhlar, D. G.; Gagliardi, L. Multiconfiguration Pair-Density Functional Theory. *J. Chem. Theory Comput.* **2014**, *10*, 3669–3680.
- [82] Bao, J. L.; Sand, A.; Gagliardi, L.; Truhlar, D. G. Correlated-Participating-Orbitals Pair-Density Functional Method and Application to Multiplet Energy Splittings of Main-Group Divalent Radicals. *J. Chem. Theory Comput.* **2016**, *12*, 4274–4283.
- [83] Gibney, D.; Boyn, J.-N.; Mazziotti, D. A. Toward a Resolution of the Static Correlation Problem in Density Functional Theory from Semidefinite Programming. *The Journal of Physical Chemistry Letters* **2021**, *12*, 385–391, PMID: 33356286.
- [84] Slater, J. C.; Johnson, K. H. Self-Consistent-Field  $X\alpha$  Cluster Method for Polyatomic Molecules and Solids. *Phys. Rev. B* **1972**, *5*, 844–853.
- [85] Ziegler, T. Approximate density functional theory as a practical tool in molecular energetics and dynamics. *Chemical Reviews* **1991**, *91*, 651–667.
- [86] Tschinke, V.; Ziegler, T. On the different representations of the hole-correlation functions in the Hartree–Fock and the Hartree–Fock–Slater methods and their influence on bond energy calculations. *The Journal of Chemical Physics* **1990**, *93*, 8051–8060.
- [87] Zhang, D.; Truhlar, D. G. Unmasking Static Correlation Error in Hybrid Kohn–Sham Density Functional Theory. *Journal of Chemical Theory and Computation* **2020**, *16*, 5432–5440, PMID: 32693604.
- [88] Gritsenko, O. V.; Schipper, P. R. T.; Baerends, E. J. Exchange and correlation energy in density functional theory: Comparison of accurate density functional theory quantities with traditional Hartree–Fock based ones and generalized gradient approximations for the molecules Li<sub>2</sub>, N<sub>2</sub>, F<sub>2</sub>. *The Journal of Chemical Physics* **1997**, *107*, 5007–5015.

# Benchmarking and contrasting exchange-correlation functional differences in response to static correlation in unrestricted Kohn-Sham and a hybrid 1-electron reduced density matrix functional theory

Daniel Gibney and Jan-Niklas Boyn

*Department of Chemistry, University of Minnesota, Minneapolis, Minnesota 55455, United States*

(Dated: Submitted April 14, 2025)

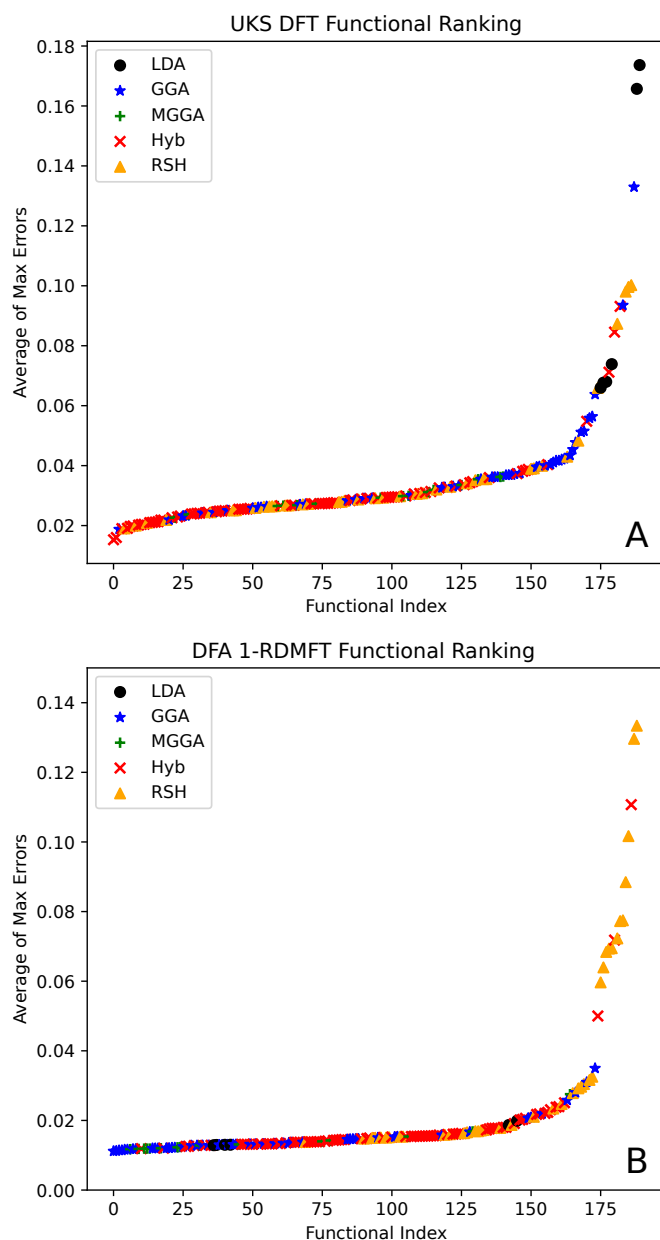


FIG. S1: Plots the functional rankings for UKS DFT (A) and DFA 1- RDMFT (B). The functionals are ranked in order of increasing average of max errors.

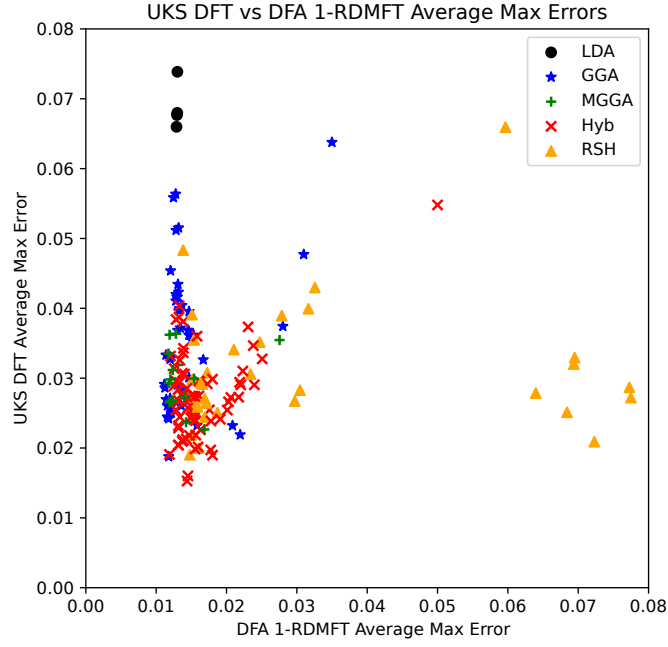


FIG. S2: Comparison between average max error from UKS DFT and DFA 1-RDMFT for the majority of functionals investigated in this work.

System	Functional			
	B3LYP	PBE	SCAN	TPSS
C <sub>2</sub>	0.257	0.264	0.256	0.263
CN	0.306	0.310	0.304	0.310
CO	0.300	0.305	0.298	0.304
F <sub>2</sub>	0.366	0.369	0.364	0.367
N <sub>2</sub>	0.340	0.345	0.338	0.345
NO	0.360	0.366	0.360	0.365
S <sub>2</sub>	0.195	0.201	0.197	0.201
SiO	0.242	0.246	0.240	0.245

TABLE S1: Optimal  $\tilde{w}$  values for each functional with 100% HF exchange.

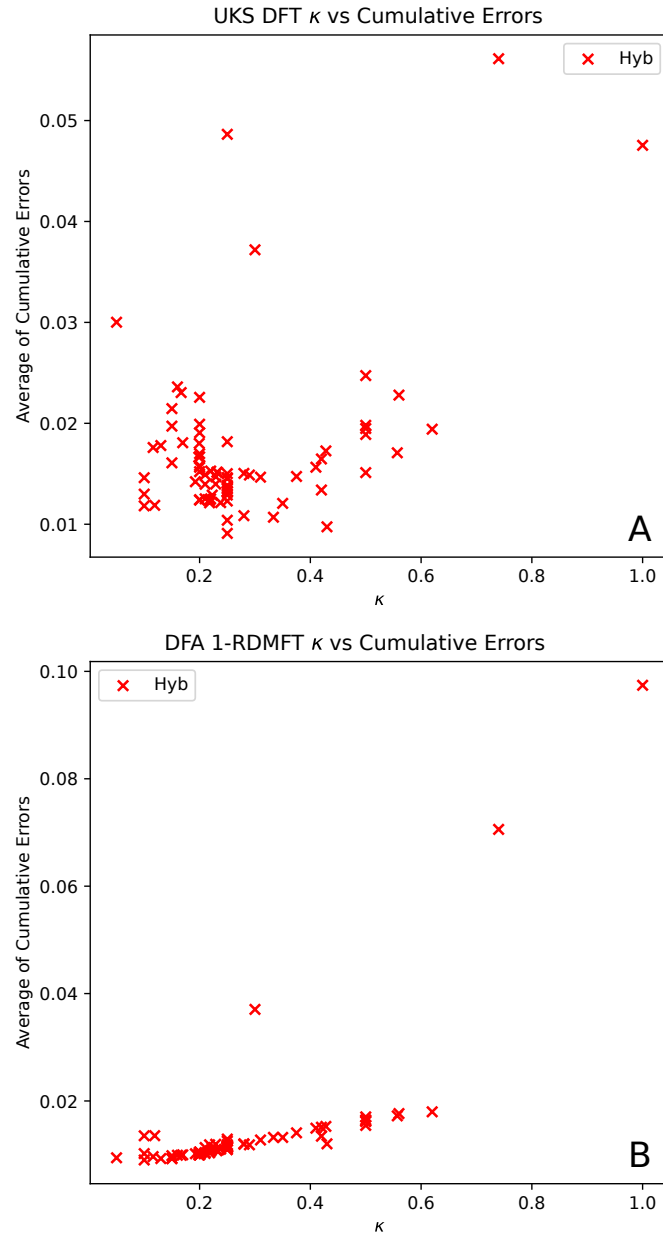


FIG. S3: Comparison between average cumulative error from UKS DFT and DFA 1-RDMFT with  $\kappa$  for the hybrid functionals investigated in this work.



Functional	Optimal $\kappa$	DFA 1-RDMFT			UKS-DFT		
		Functional Index	Average Errors		Functional Index	Average Errors	
			Max	Cumulative		Max	Cumulative
gga_xc_mohlyp2	0.0741	134	0.0158	0.0129	28	0.0232	0.0129
gga_xc_hcth_p76	0.0776	128	0.0153	0.0124	141	0.0362	0.0249
gga_xc_th_fcfo	0.0839	146	0.0219	0.0143	53	0.0219	0.0143
gga_xc_mohlyp	0.0840	122	0.0153	0.012	145	0.0362	0.0272
gga_xc_th2	0.0847	113	0.0147	0.0116	137	0.0301	0.0234
gga_xc_th3	0.0867	76	0.0138	0.0106	120	0.0283	0.0204
gga_xc_beefvdw	0.0868	15	0.0122	0.009	107	0.025	0.0188
gga_xc_xlyp	0.0870	95	0.015	0.0112	153	0.0355	0.0296
gga_xc_pbelyp1w	0.0890	80	0.0147	0.0107	162	0.0395	0.0334
gga_xc_ncap	0.0890	106	0.0147	0.0115	152	0.0362	0.0296
gga_xc_th_fco	0.0893	137	0.0209	0.0132	74	0.0232	0.0156
gga_xc_th1	0.0893	65	0.013	0.0104	122	0.029	0.0206
gga_xc_opwlyp_d	0.0902	87	0.0146	0.011	155	0.0368	0.0308
gga_xc_oblyp_d	0.0903	84	0.0145	0.0109	156	0.0369	0.0308
gga_x_chachiyogga_c_chachiyog	0.0905	73	0.0134	0.0105	149	0.0372	0.0287
gga_xc_b97_d	0.0915	27	0.0121	0.0093	114	0.0263	0.0196
gga_xc_opbe_d	0.0918	63	0.0136	0.0103	158	0.0404	0.0321
mgga_x_pkzbgga_c_pkzbg	0.0920	68	0.0128	0.0104	146	0.0364	0.0278
gga_xc_edf1	0.0924	21	0.012	0.0092	142	0.033	0.025
gga_xc_th4	0.0928	8	0.0116	0.0087	98	0.026	0.018
mgga_xc_tpsslyp1w	0.0931	72	0.014	0.0105	134	0.0273	0.0229
gga_xc_hcth_93	0.0937	5	0.0114	0.0085	90	0.027	0.0171
gga_xc_pbe1w	0.0938	40	0.0132	0.0098	159	0.0397	0.0323
gga_x_xpbe_gga_c_xpbe	0.0938	37	0.0131	0.0097	151	0.0369	0.0294
gga_xc_th_fc	0.0939	168	0.035	0.0254	175	0.0638	0.0467
gga_x_pbe_mol_gga_c_pbe_mol	0.0940	39	0.0132	0.0097	164	0.0423	0.0336
gga_xc_b97_3c	0.0942	23	0.012	0.0092	116	0.0271	0.0198
gga_x_apbe_gga_c_apbe	0.0948	38	0.0131	0.0097	168	0.0434	0.0344
gga_xc_hcth_147	0.0958	2	0.0112	0.0085	126	0.0291	0.0208
gga_xc_b97_gga1	0.0958	14	0.012	0.009	86	0.0258	0.0168
gga_xc_hcth_120	0.0960	4	0.0112	0.0085	124	0.0286	0.0207
gga_xc_hcth_407p	0.0961	6	0.012	0.0086	130	0.0327	0.0223
gga_xc_mpwlyp1w	0.0968	166	0.028	0.022	157	0.0374	0.0312
gga_xc_hcth_407	0.0969	3	0.0118	0.0085	63	0.0242	0.0148
gga_x_pbe_gga_c_pbe	0.0970	34	0.013	0.0097	166	0.0416	0.0337
gga_x_pbe_gaussian_gga_c_pbe_gaussian	0.0970	35	0.013	0.0097	165	0.0416	0.0337
gga_x_pw91_gga_c_pw91	0.0976	31	0.0128	0.0096	160	0.0411	0.0326
gga_x_rge2_gga_c_rge2	0.0991	42	0.0128	0.0098	161	0.042	0.0326
mgga_xc_otps_d	0.0999	147	0.0168	0.0149	80	0.0226	0.0159
mgga_x_tpssmgga_c_tpss	0.1002	30	0.0124	0.0095	138	0.0312	0.0236
gga_x_pbeint_gga_c_pbeint	0.1007	36	0.0128	0.0097	170	0.0512	0.0406
gga_x_am05_gga_c_am05	0.1017	22	0.0125	0.0092	173	0.0559	0.043
gga_x_pbe_fegga_c_pbe_feg	0.1020	54	0.0132	0.01	172	0.0515	0.0424
gga_x_gam_gga_c_gam	0.1020	11	0.0131	0.0088	118	0.0319	0.0198
gga_xc_kt1	0.1023	145	0.0167	0.0143	147	0.0326	0.0281
mgga_x_revtpssmgga_c_revtpss	0.1023	29	0.0123	0.0094	125	0.0268	0.0207
mgga_x_revtpmmgga_c_revtpm	0.1025	13	0.0119	0.0088	148	0.0362	0.0286
mgga_x_tmmgga_c_tm	0.1029	7	0.0118	0.0087	144	0.0335	0.0259
gga_xc_kt3	0.1033	9	0.0116	0.0088	93	0.0245	0.0176
gga_x_sg4_gga_c_sg4	0.1034	12	0.012	0.0088	167	0.0454	0.0338
gga_x_n12_gga_c_n12	0.1035	19	0.0118	0.0091	12	0.0188	0.012
gga_x_pbe_sol_gga_c_pbe_sol	0.1040	32	0.0128	0.0096	174	0.0564	0.0445
gga_xc_hcth_p14	0.1043	1	0.0114	0.0084	131	0.0333	0.0225
hyb_gga_xc_mpwlyp1m	0.1048	28	0.0128	0.0094	154	0.0384	0.03
gga_xc_kt2	0.1101	83	0.0136	0.0109	123	0.026	0.0206
lda_xc_corrksdt	0.1111	55	0.013	0.01	183	0.0739	0.0588
lda_xc_gdsmfb	0.1111	53	0.013	0.01	180	0.068	0.0535
lda_xc_ksdt	0.1113	51	0.013	0.01	179	0.0677	0.0526
lda_xc_teter93	0.1118	45	0.0129	0.01	178	0.066	0.051
mgga_x_m06_lm_gga_c_m06_l	0.1123	10	0.0118	0.0088	96	0.0293	0.0177
mgga_x_m11_lm_gga_c_m11_l	0.1125	133	0.0163	0.0128	78	0.0293	0.0158
gga_xc_th_fl	0.1147	74	0.0133	0.0105	150	0.04	0.0289
mgga_x_r2scan01mgga_c_r2scan01	0.1160	17	0.0119	0.009	88	0.0266	0.0169
mgga_x_r2scanmgga_c_r2scan	0.1162	18	0.0119	0.009	87	0.0265	0.0168
mgga_x_rscanmgga_c_rscan	0.1164	20	0.012	0.0091	109	0.0298	0.0189

Functional	Optimal $\kappa$	DFA 1-RDMFT			UKS-DFT		
		Functional Index	Average Errors		Functional Index	Average Errors	
			Max	Cumulative		Max	Cumulative
hyb_mgga_xc_x1b95	0.1174	175	0.05	0.0371	169	0.0548	0.0372
mgga_xc_hle17	0.1259	161	0.0275	0.0173	128	0.0355	0.0215
mgga_x_mn15_lmghga_c_mn15_1	0.1268	75	0.0143	0.0105	41	0.0237	0.0138
lda_xc_lp_a	0.1275	127	0.0187	0.0124	189	0.1657	0.1407
hyb_gga_xc_o3lyp	0.1285	33	0.0129	0.0096	94	0.0295	0.0176
gga_x_q2dgga_c_q2d	0.1297	157	0.0207	0.0167	187	0.0935	0.0767
hyb_mgga_xc_tpssh	0.1302	16	0.0119	0.009	10	0.0191	0.0118
hyb_gga_xc_whoeb0	0.1321	176	0.0597	0.0445	171	0.0659	0.0419
mgga_x_rev06_lmghga_c_rev06_1	0.1329	97	0.0154	0.0113	69	0.0299	0.0151
lda_xc_lp_b	0.1336	139	0.0199	0.0133	190	0.1736	0.1427
hyb_mgga_xc_revtpssh	0.1347	141	0.0156	0.0135	56	0.0239	0.0146
hyb_mgga_xc_tpss1kcis	0.1364	25	0.0125	0.0093	97	0.0289	0.0178
hyb_gga_xc_b3lyps	0.1368	24	0.012	0.0093	127	0.0332	0.0215
hyb_gga_xc_b97_1p	0.1381	41	0.0128	0.0098	81	0.0255	0.0161
hyb_mgga_xc_mpw1kcis	0.1382	26	0.0126	0.0093	115	0.0314	0.0197
gga_xc_hle16	0.1400	169	0.031	0.0254	143	0.0477	0.0259
hyb_gga_xc_wp04	0.1404	142	0.018	0.0135	11	0.0299	0.0119
hyb_mgga_xc_r2scanh	0.1439	59	0.0139	0.0102	29	0.0211	0.013
hyb_gga_xc_edf2	0.1474	47	0.0134	0.01	102	0.0326	0.0181
hyb_gga_xc_sb98_1c	0.1494	57	0.0132	0.0102	52	0.0232	0.0142
hyb_gga_xc_b97	0.1499	61	0.0132	0.0102	44	0.0229	0.014
hyb_gga_xc_b3lyp3	0.1504	49	0.0132	0.01	20	0.0204	0.0124
hyb_gga_xc_b3lyp5	0.1505	50	0.0132	0.01	19	0.0204	0.0124
hyb_gga_xc_hpbeint	0.1507	44	0.0133	0.0099	136	0.0387	0.023
hyb_gga_xc_b3lyp	0.1507	52	0.0132	0.01	75	0.0267	0.0156
hyb_gga_xc_b1wc	0.1508	43	0.0133	0.0099	139	0.0403	0.0236
hyb_gga_xc_sb98_1b	0.1516	58	0.0137	0.0102	99	0.0307	0.018
hyb_gga_xc_revb3lyp	0.1523	56	0.0133	0.01	89	0.0294	0.017
hyb_gga_xc_hse06	0.1527	92	0.015	0.0111	49	0.0264	0.0141
hyb_gga_xc_b3lyp_mcm1	0.1528	46	0.0131	0.01	84	0.0283	0.0167
hyb_gga_xc_hjs_pbe	0.1530	94	0.015	0.0112	9	0.0219	0.0114
hyb_gga_xc_hse03	0.1539	93	0.0152	0.0112	48	0.0265	0.014
hyb_gga_xc_mb3lyp_rc04	0.1544	62	0.0138	0.0103	119	0.0336	0.0199
hyb_gga_xc_b97_1	0.1554	67	0.0134	0.0104	65	0.0244	0.0149
hyb_gga_xc_b3pw91	0.1555	71	0.0139	0.0105	72	0.0276	0.0152
hyb_gga_xc_b3p86	0.1559	60	0.0136	0.0102	79	0.0276	0.0158
hyb_gga_xc_hjs_b97x	0.1560	109	0.0151	0.0115	82	0.0298	0.0162
hyb_gga_xc_hapbe	0.1567	69	0.0139	0.0104	132	0.0381	0.0226
hyb_gga_xc_x3lyp	0.1569	64	0.0137	0.0103	14	0.021	0.0121
hyb_gga_xc_mpw3pw	0.1571	70	0.014	0.0105	85	0.0306	0.0167
hyb_gga_xc_b3p86_nwchem	0.1576	66	0.0139	0.0104	110	0.0343	0.0191
hyb_gga_xc_sb98_2c	0.1580	81	0.0138	0.0108	21	0.0212	0.0125
hyb_gga_xc_b97_2	0.1584	101	0.0149	0.0113	22	0.0243	0.0125
hyb_gga_xc_hjs_pbe_sol	0.1588	98	0.0154	0.0113	103	0.0355	0.0181
hyb_gga_xc_hse_sol	0.1588	99	0.0154	0.0113	100	0.0355	0.018
hyb_gga_xc_mpw3lyp	0.1589	117	0.0156	0.0118	17	0.0218	0.0123
hyb_mgga_xc_pbe1kcis	0.1602	77	0.0144	0.0106	73	0.0285	0.0153
hyb_gga_xc_sb98_2a	0.1621	82	0.0141	0.0108	71	0.0268	0.0152
hyb_gga_xc_b3lyp_mcm2	0.1627	100	0.0154	0.0113	26	0.0248	0.0129
hyb_gga_xc_sb98_2b	0.1635	90	0.0143	0.011	15	0.0213	0.0121
hyb_gga_xc_sb98_1a	0.1643	120	0.0161	0.0119	46	0.0275	0.014
hyb_gga_xc_b1lyp	0.1645	86	0.0145	0.0109	1	0.016	0.0091
gga_x_hcth_agga_c_hcth_a	0.1649	165	0.0258	0.0201	188	0.133	0.0936
hyb_gga_xc_hse12s	0.1652	143	0.0187	0.0139	77	0.0251	0.0158
hyb_gga_xc_mpw1lyp	0.1658	88	0.0147	0.011	16	0.0218	0.0123
hyb_gga_xc_apf	0.1658	89	0.0148	0.011	60	0.0273	0.0147
hyb_gga_xc_camy_pbeh	0.1676	149	0.0179	0.015	185	0.1002	0.0636
hyb_gga_xc_relpbe0	0.1688	79	0.0145	0.0107	70	0.0257	0.0151
hyb_gga_xc_hse12	0.1694	130	0.0169	0.0125	36	0.0244	0.0134
hyb_gga_xc_case21	0.1700	96	0.0152	0.0112	55	0.0274	0.0146
hyb_gga_xc_cap0	0.1703	115	0.0151	0.0117	43	0.0246	0.0139
hyb_gga_xc_pbe_molb0	0.1707	103	0.0154	0.0114	32	0.025	0.0132
hyb_gga_xc_b1pw91	0.1707	114	0.0154	0.0116	30	0.0241	0.0132
hyb_gga_xc_pbe_mol0	0.1708	108	0.0154	0.0115	33	0.0248	0.0133

Functional	Optimal $\kappa$	DFA 1-RDMFT			UKS-DFT		
		Functional Index	Average Errors		Functional Index	Average Errors	
			Max	Cumulative		Max	Cumulative
hyb_gga_xc_apbe0	0.1714	107	0.0155	0.0115	38	0.0255	0.0136
hyb_gga_xc_mpw1pw	0.1721	111	0.0156	0.0116	37	0.0251	0.0135
hyb_gga_xc_mpw1pbe	0.1724	112	0.0155	0.0116	5	0.0199	0.0104
hyb_gga_xc_pbe0	0.1726	104	0.0155	0.0114	57	0.0273	0.0146
hyb_gga_xc_pbeh	0.1731	105	0.0155	0.0114	54	0.0274	0.0145
hyb_mgga_xc_b86b95	0.1746	119	0.0161	0.0119	67	0.0296	0.015
hyb_mgga_xc_pw6b95	0.1751	124	0.0163	0.012	8	0.0226	0.0108
hyb_mgga_xc_tpss0	0.1753	118	0.016	0.0119	27	0.0202	0.0129
hyb_mgga_xc_pw86b95	0.1768	116	0.0162	0.0118	64	0.0295	0.0149
hyb_gga_xc_pbe_sol0	0.1781	102	0.0158	0.0114	104	0.036	0.0182
hyb_gga_xc_mcam_b3lyp	0.1838	85	0.0148	0.0109	6	0.019	0.0104
hyb_mgga_xc_r2scan0	0.1856	135	0.0178	0.0129	66	0.0239	0.015
hyb_mgga_xc_mpw1b95	0.1858	132	0.0173	0.0127	58	0.0292	0.0147
hyb_gga_xc_cam_pbeh	0.1874	153	0.021	0.0157	129	0.0341	0.0218
hyb_mgga_xc_b0kcis	0.1889	131	0.0178	0.0125	177	0.0846	0.0486
hyb_mgga_xc_xb1k	0.1912	123	0.0144	0.012	2	0.0153	0.0097
hyb_gga_xc_blyp35	0.1952	136	0.0178	0.0132	13	0.0197	0.0121
hyb_gga_xc_pbe0_13	0.1984	138	0.018	0.0132	7	0.019	0.0107
hyb_gga_xc_wc04	0.2007	184	0.0718	0.0706	181	0.0931	0.0561
hyb_gga_xc_camh_b3lyp	0.2081	110	0.016	0.0115	3	0.02	0.0099
hyb_gga_xc_pbe38	0.2109	144	0.0191	0.0141	61	0.0241	0.0147
hyb_gga_xc_b97_k	0.2114	140	0.0176	0.0134	35	0.0255	0.0134
hyb_mgga_xc_mpwkcis1k	0.2174	148	0.0201	0.0149	76	0.0254	0.0157
hyb_mgga_xc_bb1k	0.2182	150	0.0203	0.0151	83	0.0266	0.0165
hyb_gga_xc_tuned_cam_b3lyp	0.2200	48	0.0138	0.01	163	0.0483	0.0336
hyb_gga_xc_mpw1k	0.2262	151	0.0206	0.0153	92	0.0272	0.0173
hyb_gga_xc_wb97x_d3	0.2347	181	0.0723	0.0662	4	0.0209	0.01
hyb_gga_xc_cam_b3lyp	0.2383	125	0.0171	0.0122	23	0.0265	0.0126
hyb_gga_xc_bhandhlyp	0.2409	154	0.0219	0.0162	113	0.0294	0.0195
hyb_gga_xc_b50501yp	0.2423	155	0.022	0.0163	108	0.029	0.0189
hyb_gga_xc_pbe50	0.2487	156	0.0223	0.0165	117	0.031	0.0198
hyb_mgga_xc_r2scan50	0.2541	158	0.0231	0.017	140	0.0373	0.0247
hyb_gga_xc_bhandh	0.2554	152	0.0217	0.0154	68	0.0273	0.0151
hyb_gga_xc_lc_wpbe08_whs	0.2558	186	0.1017	0.0919	59	0.0267	0.0147
hyb_gga_xc_lc_wpbeh_whs	0.2572	188	0.1296	0.1171	105	0.0279	0.0184
hyb_gga_xc_cam_qtp_01	0.2592	183	0.0775	0.0692	25	0.0272	0.0129
hyb_gga_xc_lc_wpbe_whs	0.2599	182	0.0773	0.0691	51	0.0287	0.0142
hyb_gga_xc_camy_blyp	0.2623	189	0.1334	0.1205	182	0.0873	0.0563
hyb_gga_xc_wb97x_d	0.2637	126	0.0169	0.0123	40	0.0271	0.0137
hyb_gga_xc_lrc_wpbeh	0.2644	121	0.0166	0.012	50	0.0291	0.0142
hyb_gga_xc_lc_blypr	0.2644	170	0.0279	0.0259	95	0.039	0.0176
hyb_gga_xc_lc_pbeop	0.2650	173	0.0316	0.031	101	0.0399	0.018
hyb_gga_xc_pbe_2x	0.2668	162	0.0238	0.0177	133	0.0347	0.0228
hyb_gga_xc_lc_blyp	0.2678	174	0.0326	0.0324	121	0.043	0.0205
hyb_gga_xc_kmlyp	0.2692	159	0.024	0.0172	91	0.0291	0.0171
hyb_gga_xc_wb97x	0.2729	172	0.0297	0.0279	34	0.0267	0.0133
hyb_mgga_xc_lc_tmlyp	0.2730	91	0.0159	0.0111	18	0.0259	0.0123
hyb_gga_xc_lrc_wpbe	0.2762	78	0.0151	0.0107	106	0.0391	0.0187
hyb_gga_xc_lc_wpbe	0.2808	177	0.064	0.0535	42	0.0279	0.0138
hyb_gga_xc_rcam_b3lyp	0.2811	185	0.0885	0.08	24	0.0263	0.0128
hyb_gga_xc_lcy_pbe	0.2839	190	0.1956	0.1653	186	0.0996	0.0645
hyb_gga_xc_wb97	0.2857	171	0.0305	0.0276	39	0.0283	0.0137
hyb_gga_xc_qtp17	0.2877	163	0.0251	0.018	112	0.0328	0.0194
hyb_gga_xc_cam_qtp_02	0.2899	178	0.0684	0.0567	31	0.0251	0.0132
hyb_gga_xc_lc_bop	0.2934	180	0.0694	0.0579	62	0.032	0.0147
hyb_gga_xc_lc_qtp	0.2975	179	0.0695	0.0575	47	0.033	0.014
hyb_gga_xc_lb07	0.3190	129	0.0173	0.0124	45	0.0308	0.014
hyb_gga_xc_cam_qtp_00	0.3208	164	0.0247	0.0181	135	0.0352	0.023
hyb_gga_xc_hflyp	0.3336	187	0.1107	0.0974	176	0.0712	0.0475
hyb_gga_xc_lc_wpbesol_whs	0.3515	160	0.0234	0.0172	111	0.0306	0.0194
hyb_gga_xc_lcy_blyp	0.3886	167	0.0292	0.023	184	0.0981	0.06

TABLE S2: Optimal  $\kappa$  values and related functional indices and errors obtained in this work.

	N <sub>2</sub> 1.1 Å			N <sub>2</sub> 3.0 Å		
	PBE	PBE 1-RDMFT	Ratio	PBE	PBE 1-RDMFT	Ratio
dz	0.040	0.155	3.886	0.040	0.167	4.167
tz	0.062	0.289	4.682	0.061	0.300	4.900
qz	0.122	0.626	5.143	0.129	0.617	4.791
5z	0.312	1.330	4.267	0.314	1.298	4.139

TABLE S3: Average time, in seconds, for each SCF iteration from UKS PBE and PBE 1-RDMFT in various basis sets and their ratio, considering N<sub>2</sub> in varying sized basis sets at 1.1 Å and 3.0 Å. All PBE 1-RDMFT calculations required 6 iterations to converge the energy to  $< 1e-8$ . PBE UKS calculations at 1.1 Å required 6 cycles to converge and 8 cycles at 3.0 Å

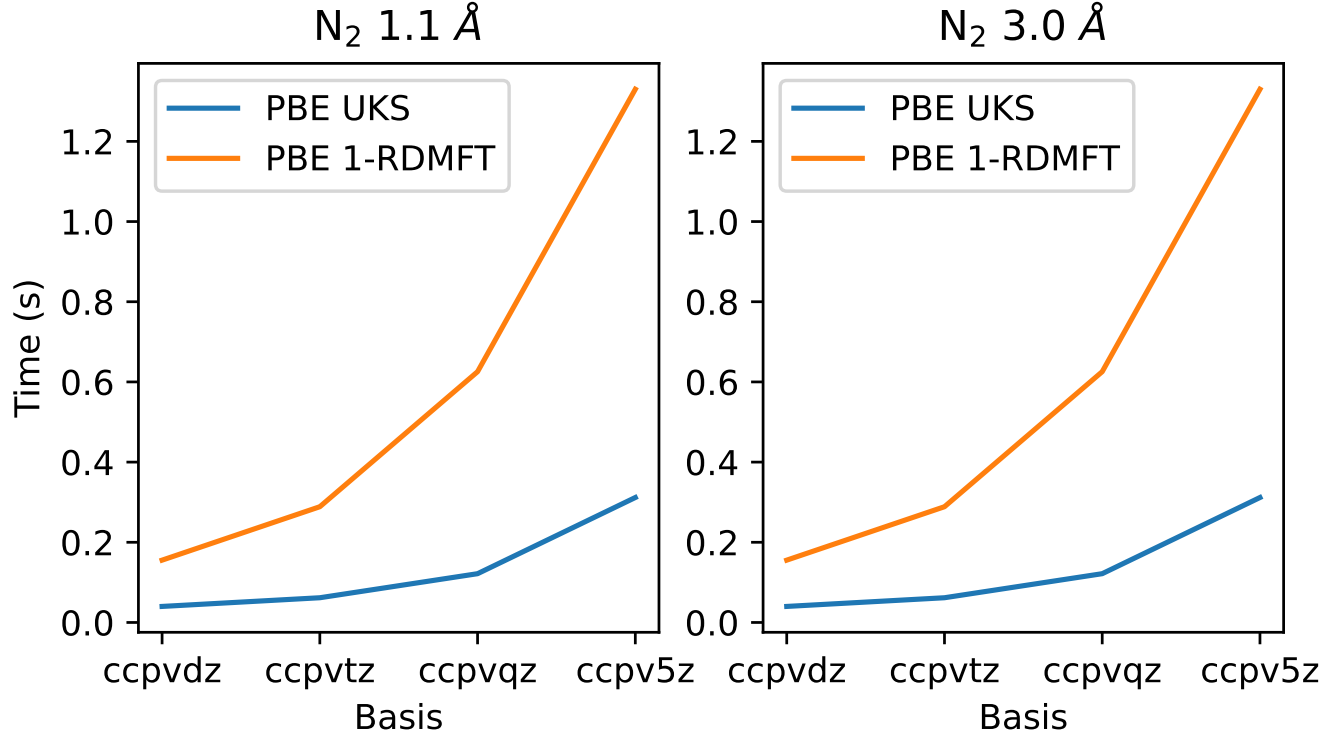


FIG. S4: Timing comparisons between PBE UKS and PBE 1-RDMFT with N<sub>2</sub> at 1.1 and 3.0 interatomic distances in the cc-pvdz, cc-pvtz, cc-pvqz, and cc-pv5z basis sets.

Table S3 and Figure S4 show example timing data from UKS DFT and DFA 1-RDMFT in a variety of basis sets using the PySCF package. These results demonstrate comparable scaling with basis set size across UKS-DFT and DFA 1-RDMFT, with an additional prefactor arising from the SDP in the case of the latter. We note that in strongly correlated systems the DFA 1-RDMFT framework tends to converge in fewer cycles than UKS DFT. This is evident in these examples: PBE 1-RDMFT converged after six cycles, irrespective of the basis set used or the bond length considered, while UKS PBE required 6 cycles to converge for all basis sets at the 1.1 Å bond length, but required 8 cycles at the 3.0 Å bond length.